Investigating oxygen fugacity changes as results of subduction metamorphism and metasomatism

Zexing Zheng

GEOL394

04/28/2020

Advisors: Dr. Sarah Penniston-Dorland, Will Hoover and Kayleigh Harvey

Abstract

Arc magmas are more oxidized compared to other magmas, although the cause of this high oxygen fugacity is poorly understood. Previous studies have suggested that subducted oxidized oceanic crust transfers its oxidation potential through fluids to the arc magma source in subduction zones causing high oxygen fugacity in arc magmas (Holycross and Cottrell, 2020). Vanadium is an oxygen fugacity-sensitive trace element and can be used as an indicator of oxygen fugacity. Previous studies proposed a relationship between the vanadium ratio of rutile to omphacite and the oxygen fugacity based on the results of closed system eclogite experiments. At higher oxygen fugacity (oxidized conditions), rutile is more enriched in vanadium. In contrast, rutile will be less enriched in vanadium relative to omphacite in more reduced systems. In this study, the empirical relationship between vanadium partitioning in rutile and omphacite was compared between mineral pairs in eclogites from the Franciscan Complex (CA) and the Monviso Metaophiolite Complex (Italy) to test the effect of prograde metamorphism and metasomatic alteration on oxidation state. Analyses on the Franciscan Complex sample shows a clear difference in vanadium partitioning in rutile between the inclusion and matrix phases that formed under different metamorphic stages. However, vanadium partitioning in omphacite from the same sample does not show distinct differences, and the vanadium ratio based on these data also does not show apparent differences. The Monviso Complex sample shows similar vanadium partitioning patterns in rutile and omphacite, but a distinct vanadium ratio that decreased from the unaltered to altered regions. Factors such as temperatures and the chemical equilibrium could potentially affect vanadium partitioning; however, estimated temperatures and major element differences between two phases (regions) in two samples do not suggest any relationships between these factors and vanadium partitioning. By excluding these mechanisms, the only factor, oxygen fugacity from the fluid, had to have caused changes in vanadium partitioning in the Monviso sample. Comparing textural relationships in the Franciscan Complex sample, prograde and retrograde minerals such as glaucophane that surrounded by omphacite matrix and deposited along with garnet fractures infer oxygen fugacity had changed before and after both phases crystallized and resulted in a low oxygen fugacity environment recorded by inclusion eclogite facies minerals.

Introduction

Oxygen fugacity (fO₂) governs the partitioning of elements and mass transfer during metasomatism in chemical systems within the Earth. It refers to the potential of elements to oxidize or reduce their valence state. Under very low oxygen fugacity conditions, such as Earth's core, metallic elements such as iron (Fe) exist in their metal form. In contrast, metallic elements under higher oxygen fugacity environments are in oxidized states, such as Fe⁺² and Fe⁺³(Frost, 1991). Reactions listed in Table 1 are called "buffers," each of which represents an equilibrium reaction that takes place under different oxygen fugacity conditions. The absolute value of oxygen fugacity for any buffer changes under different pressure-temperature conditions (Figure 1).

Table 1. Examples of oxygen fugacity buffers

Chemical equations	Oxidation states
2 Fe + SiO2 + O2 = Fe2SiO4 (QIF)	Fe^0 — Fe^{2+}
$3 \text{ Fe}_2 \text{SiO}_4 + \text{O}_2 = 2 \text{ Fe}_3 \text{O}_4 + 3 \text{ SiO}_2 \text{ (FMQ)}$	Fe^{2+} — $Fe^{8/3+}$
$4 \text{ Fe}_3\text{O}_4 + \text{O}_2 = 6 \text{ Fe}_2\text{O}_3 \text{ (MH)}$	$Fe^{8/3+}$ — Fe^{3+}

Not all buffers listed. QIF, quartz-iron-fayalite; FMQ, fayalite-magnetite-quartz; MH, magnetite-hematite. Source: Frost, (1991).

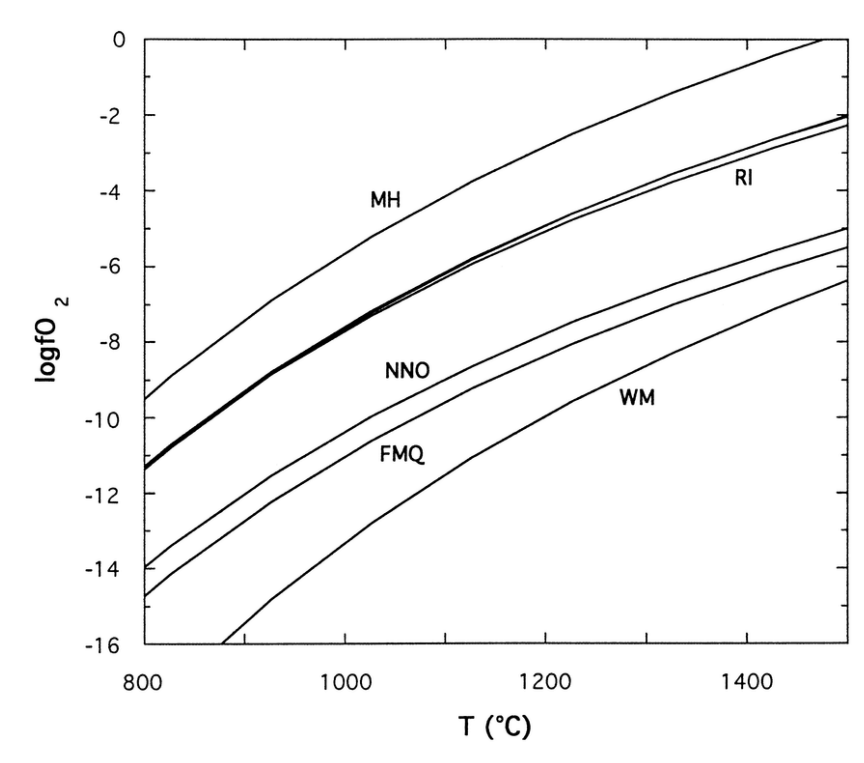


Figure 1. log fO2 versus T of some oxygen buffers reaction at P = 1 bar. NNO, nickel-nickel oxide; WM, wustite-magnetite; RI, rutile-ilmenite. Source: Zhao et al., (1999).

Evidence shows that arc basalts (basalts generated in arc volcanoes above subduction zones) have higher oxygen fugacities in comparison with other types of basalt, yet the cause is not clearly defined (Kelley and Cottrell, 2012). One plausible explanation presented is that the oxidization potential is transferred from a subducting slab to the arc magma via fluids (Kelley and Cottrell, 2009). As a result, the oxygen fugacity in the subducting slab should decrease throughout subduction as more oxidized fluids are released from the slab. A recent study on mantle wedge orthopyroxene found a positive correlation between H₂O concentration in mantle wedge orthopyroxene and oxygen fugacity and supports this explanation (Tollan & Hermann, 2019).

Elements that naturally exist in multiple valence states, such as iron or vanadium, can be used as an indicator of the oxygen fugacity recorded by natural rocks. Eclogites are mafic metamorphic rocks mainly containing garnets and clinopyroxenes that form in subduction zones within a high-pressure/low-temperature conditions. The distribution of redox-sensitive trace elements in minerals within eclogites, such as vanadium, could record the change in oxygen fugacity during subduction (Liu et al.,2014).

Minerals containing V, such as pyroxene and rutile in eclogites, record the oxygen fugacity record the oxygen fugacity of the rock as it experiences metamorphism (Aulbach and Stagno, 2016). At low oxygen fugacity ($\log fO_2=QFM-3$), omphacite will be more V^{3+} is preferably formed and substitutes for aluminum (Al³⁺) in omphacite. In contrast, under oxidizing conditions V^{4+} replaces titanium (Ti⁴⁺) in rutile. Holycross & Cottrell (2020) conducted closed system experiments on eclogite samples under pressures of 1.2-2 GPa, temperatures between 850-1050°C, and oxygen fugacities between $\log fO2=QFM-3$ and QFM+5. The study found a correlation between rutile/omphacite partitioning of V and oxygen fugacity.

In this study, I investigate the changes in V content of rutile and omphacite and assess the implications for changes in oxygen fugacity using two different approaches on two eclogites from different localities. The first approach compares the V content of earlier-formed inclusions inside of garnets with the V content of later-formed matrix minerals to investigate changes in oxygen fugacity during prograde metamorphism. The sample was used for this approach is from the Franciscan Complex, California, which has evidence for series of metamorphic events. The first hypothesis for this study is the V concentration ratio of rutile and omphacite would decrease from the inclusion to the matrix phases if the oxygen fugacity escaped from the subducting slab. The second approach investigates the V content of minerals in an unaltered metamorphic rock and compares those to the V content of the same minerals in a part of the same rock that was altered by metamorphic fluids to investigate changes in oxygen fugacity due to fluid-rock interaction. Therefore, an eclogite that from the Monviso Metaophiolite Complex, Italy records evidence of rock-fluid interaction in the form of a reaction rind was analyzed for the second approach, and it is hypothesized that the rock-fluid interaction would cause changes in the V concentration ratio of rutile and omphacite from unaltered to altered regions for the second approach.

Geologic background of samples

The Franciscan Complex eclogite

One eclogite sample for the study was collected from the Franciscan Complex at Jenner Beach near Jenner, CA, north of San Francisco (Figures 2 and 3). The Franciscan Complex formed in the Mesozoic era when the Farallon Plate subducted beneath the North American Plate. Based on Krogh et al. (1999), the Franciscan Complex has evidence for eight stages of prograde metamorphisms (continuous phases of metamorphism throughout subduction), and the metamorphic rock samples they analyzed recorded more than one stage of metamorphism. This means that this eclogite sample from the same complex has the potential to preserve variations in trace element concentration in different mineral phases throughout the metamorphic evolution: an earlier eclogite facies metamorphic stage represented by inclusions within garnets and other minerals, and a later stage in the matrix minerals. The sample followed a counter-clockwise *P-T* path, with peak metamorphic conditions of about 1.5 GPa and 560°C (Krogh et al., 1994; Figure 4). Rutile and omphacite occur both in the matrix and as coexisting inclusions in garnet. Comparing minerals and their chemical properties between different metamorphic stages could provide oxygen fugacity changes during prograde metamorphism.



Figure 2. A photo of the eclogite sample collected at Jenner Beach, Franciscan Complex, CA. Unit scale in centimeters. Credits to Dr. Sarah Penniston-Dorland.

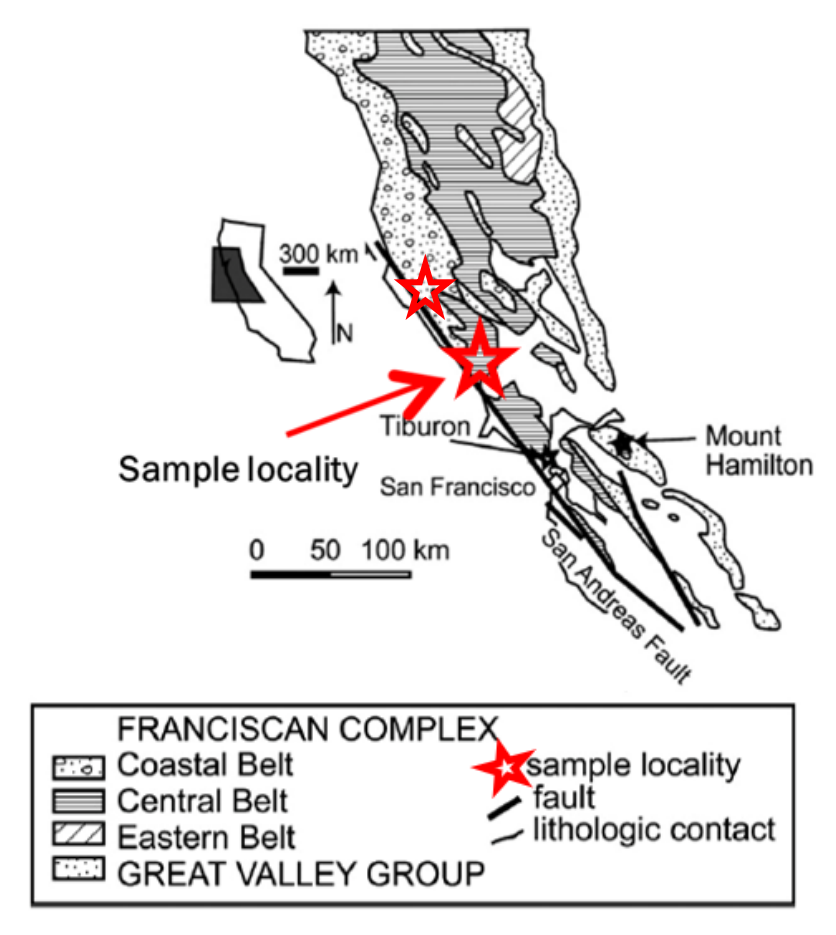


Figure 3. Geologic map of the Franciscan Complex and the sample locality. Source: Modified from Catlos and Sorensen (2003).

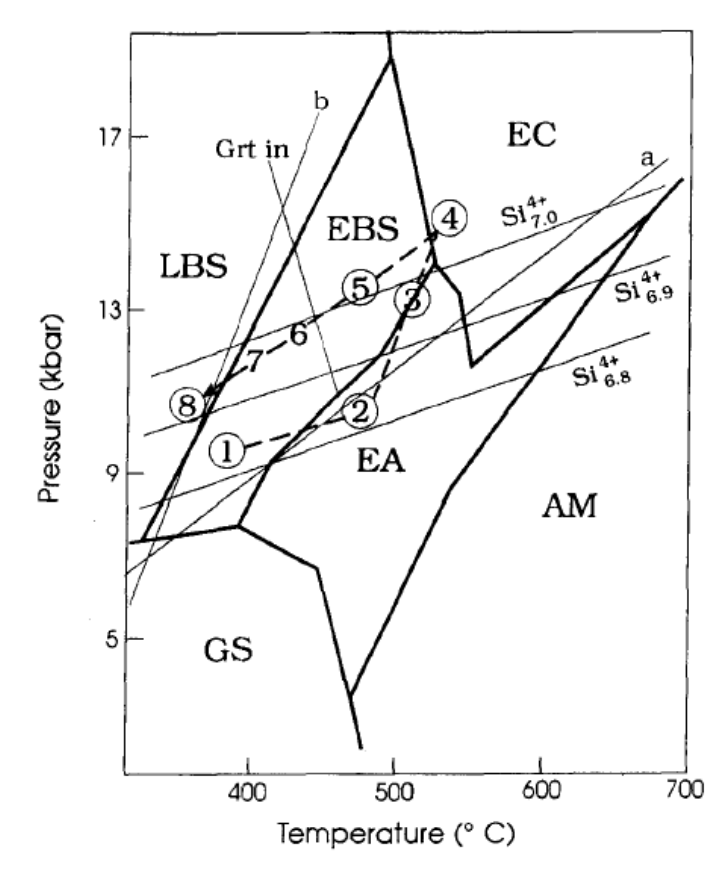


Figure 4. The counter-clockwise P-T pathway of the Franciscan Complex. Source: Krogh et al., (1994). Label 4 on the pathway is at the peak metamorphic condition.

The Monviso Metaophiolite Complex eclogite sample

Another sample was collected from within the Lower Shear Zone (LSZ) sub-unit, Lago Superiore Unit, Monviso Metaophiolite complex (W. Alps). The complex formed during convergence and subsequent collision between Adria and Europe plates during the Cretaceous period, with the closing of Jurassic Tethys ocean (Locatelli et al., 2019). The Monviso Metaophiolite Complex consists of two metamorphic units: the Monviso Unit to the west, and the Lago Superiore Unit (LSU) to the east with a peak metamorphic condition around 2.6GPa and 550°C (Angiboust et al., 2011). The Lago Superiore Unit is cut by two eclogite facies shear zones shown in the cross-section (Figure 5): one is in the Intermediate Shear Zone (ISZ), and the other is in Low Shear Zone (LSZ). The eclogite shear zone contact with serpentinites in the LSZ and was heavily metasomatized by fluid enriched in Mg, chromium (Cr), and nickel (Ni) under a *P-T* condition around 2.5GPa and 550°C which is close to the peak metamorphic condition (Angiboust et al., 2014).

The Monviso sample block was surrounded by reaction rind, however, the inner part is mostly unaltered. Therefore, minerals in two regions can provide evidence for oxygen fugacity changes due to metasomatism.

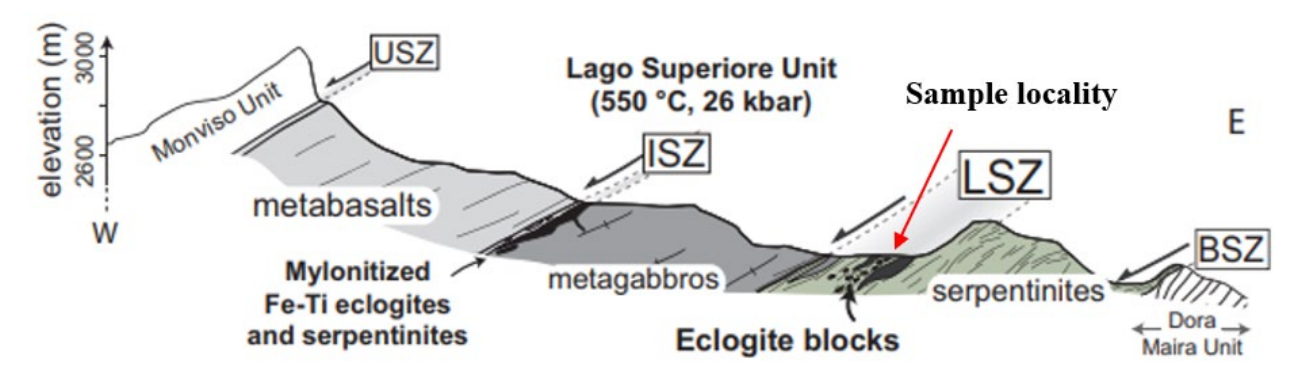


Figure 5. Monviso Complex cross-section. Source: Angiboust et al., (2014).

Methods

Rutile-omphacite pairs in different phases or regions (e.g., matrix phase and altered region) of each sample were marked out by an optical microscope and then analyzed for major elements using Energy Dispersive Spectroscopy (EDS) and wavelength dispersive spectroscopy (WDS), which both are on the electron probe micro-analyzer (EPMA). Finally, the Laser Ablation Inductively Coupled Plasma Mass Spectrometry (LA-ICP-MS) is used to determine trace-element compositions such as V and Zr, which are essential to this study. Effort was made to analyze the same location on minerals for both EPMA and LA-ICPS-MS analysis

Petrography

A Nikon Eclipse LV100 Polarizing microscope with a QImaging Micropublisher 5.0-RTV camera was used to take photomicrographs under plane-polarized light (PPL), cross-polarized light (XPL), and reflected light (RL) on each grain. For the Franciscan Complex sample, thirteen pairs of rutile and omphacite grains (six pairs in the matrix phase, seven pairs in the inclusion phase) were chosen in two phases that were as close to each other as possible (Figure 6). Matrix and inclusion phases were coded with "M" and "In", respectively. Spots for matrix analysis were selected near the rims of minerals given that they are most likely to be in chemical equilibrium.

There are two textural domains within the eclogite block from the Monviso eclogite: the unaltered region (UN) with abundant garnets and altered regions (AL) defined by garnet replacement by chlorite. Five rutile-omphacite pairs of each region were mapped out and selected for later EPMA and LA-ICP-MS analyses.

EPMA

In this study, a JEOL JXA-8900 Electron Probe Microanalyzer was utilized at the University of Maryland, in a lab operated by Dr. Philip M. Piccoli. Major element composition of phases was analyzed by using the EPMA as this information is required as the internal

standard for the LA-ICP-MS measurements. The EPMA was set up for two samples as following listed: Accelerated voltage = 15kV; cup current = 10 nA; beam diameters for rutile and omphacite are 1 and 5 microns, respectively; the detection limit for V_2O_3 is 200 ppm.

LA-ICP-MS

The LA-ICP-MS used in this study is a ThermoFinnigan Element 2, and the laser is an Nd:YAG UP213 (New Wave) infrared laser with a wavelength at 1064 nm. Five elements (V, titanium (Ti), zirconium (Zr), calcium (Ca) and silicon (Si)) are essential to this study and measured by this instrument operated by Dr. Richard Ash at the University of Maryland. Titanium and Si were used as internal standards for the correction of rutile and omphacite analyses, respectively.

Before analyzing eclogite samples, NIST610 (a glass) and R10 (nature rutile from Norway; V = 1279 ppm; Luvizotto et al. 2009) were analyzed as primary and secondary standards respectively. The calculated standard deviation based on eight analyses on the glass standard NIST 610 (Appendix 4) was used to determine the uncertainty I need both rutile and omphacite analyses in Franciscan Complex and Monviso Metaophiolite Complex eclogites. Further EPMA and LA-ICP-MS methods are discussed in Appendix 3.

Equations

In this study, the V concentration ratio (V_{ratio}) and uncertainty (δV_{ratio}) are given by

$$V_{\text{ratio}} = \frac{V_{\text{Rt}}}{V_{\text{omp}}} \tag{1a}$$

$$\delta V_{\text{ratio}} = V_{\text{ratio}} \sqrt{\left(\frac{\delta V_{\text{Rt}}}{V_{\text{Rt}}}\right)^2 + \left(\frac{\delta V_{\text{Omp}}}{V_{\text{Omp}}}\right)^2}$$
 (1b)

According to previous studies, V partitioning is affected by temperature in addition to oxygen fugacity (Holycross and Cottrell, 2020). Temperatures of eclogites from two localities were calculated according to the method and the equation from Tomkins et al. (2007)

$$T(^{\circ}C) = \frac{83.9 + 0.410P}{0.1428 - R \ln \phi} - 273 \tag{2}$$

Equation 2 determines the temperature from the Zr concentration in rutile and is valid for systems in the quartz field where both sample localities located. R is the gas constant, 0.0083144 kJ K⁻¹, P is pressure in kbar and ϕ is Zr concentration in ppm. Use the average temperature and two standard deviations as the temperature estimate for each region (phases). However, this uncertainty is much more considerable than analytical uncertainty.

Results

Mineralogy of the Franciscan Complex eclogite sample

Subhedral omphacite, euhedral garnet with omphacite and rutile inclusions, anhedral rutile, and glaucophane make up the Franciscan Complex sample. Minerals are randomly distributed in the thin section. However, rutile and omphacite grain sizes between the two phases

are different: from ~0.1 mm to 1 mm between inclusion and matrix phases (Figure 6). Some matrix rutile is surrounded by titanite rims, which suggest some minor retrogression.

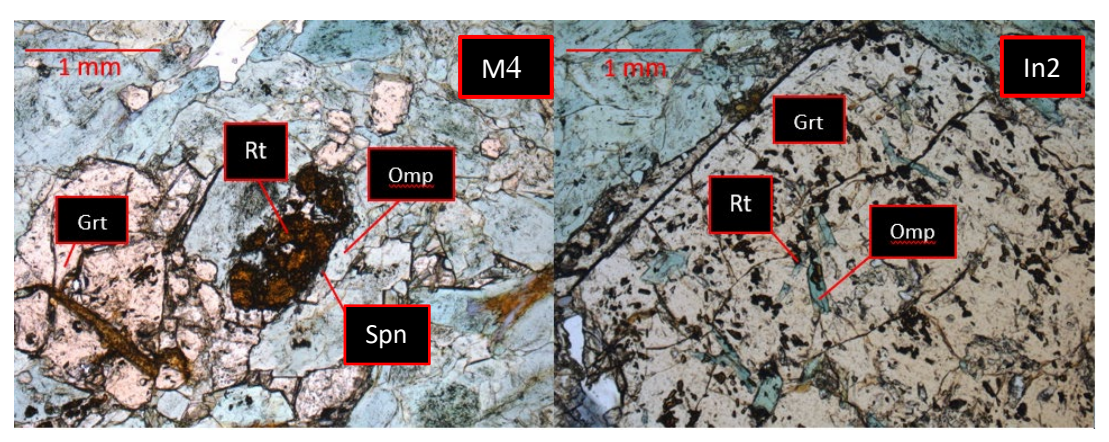


Figure 6 Examples of matrix and inclusion mineral pairs of the Franciscan Complex sample. Grt, garnet; Rt, rutile; Omp, omphacite; Spn, sphene (titanite). Mineral abbreviation source: Whitney and Evans, 2010.

Mineralogy of the Monviso Complex eclogite sample

The unaltered region of the thin section mainly consists of anhedral garnet, omphacite, and multiple rutile bands that cut through this region and enter into the altered region. The unaltered region mylonitized and, segregated by different minerals. Grain sizes of these minerals are relatively consistent, between ~0.2-0.5 mm. The altered region of the thin section consists of elongated omphacite and chlorite that vary in sizes, subhedral amphibole, sulfides, and dismembered anhedral rutile bands that extend from the unaltered region. No systematic mineral distribution is visible in the altered region, and grain sizes vary significantly from 0.05 to 1.5 mm.

Garnet pseudomorphs (Figure 7) that have been replaced by chlorite appear in the area between the two regions indicating this sample has gone through an alteration event, with chlorite as an alteration product mineral.

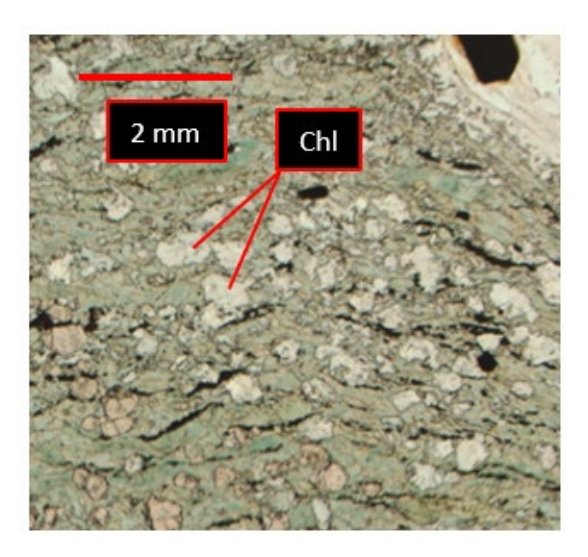


Figure 7. PPL image showing garnet pseudomorphs that have been replaced by transparent chlorite grains.

EPMA results of two samples

Thirteen rutile and omphacite pairs from the Franciscan Complex were analyzed by EPMA. These pairs contain both inclusions and matrix phases that formed during prograde-peak and peak metamorphism, respectively. Major element compositions such as Fe show differences between two phases, with a lower iron oxide average of 9.22 ± 0.367 wt% in the matrix phase, compared to the average of 12.0 ± 0.446 wt% of the same compound in the inclusion phase (Table 2).

Ten analyzed mineral pairs from Monviso Complex, with two spots on each mineral rim (four spots per mineral pair) except one omphacite that showed two shading color under backscattered image (BSE) has two analysis spots on each color region. The result shows major element composition differences between unaltered and altered regions, such as Ca, with an average of 13.7 ± 0.274 wt% and 16.1 ± 0.271 wt% respectively (Table 3). These pairs from Monviso Complex were only analyzed on mineral rims that formed in a relatively close period compared to pairs from Franciscan Complex. Therefore, there is no chemical comparability between two localities.

Table 2. Iron oxide weight percent of each analyzing Franciscan Complex omphacite point.

Franciscan Complex	FeO
Analyzing points	wt %
M1	10.05
M2	8.32
M3	8.08
M4	11.65
M5	8.69
M6	8.50
ln1	11.85
In2	12.01
In2b	12.70
In2c	12.13
In3	11.18
In4	10.98
In5	12.76
Average (Matrix)	9.22
Average (Inclusion)	11.95

Table 3. Calcium oxide weight percent of each Monviso Complex omphacite analysis spots.

Monviso Complex	CaO
Analyzing points	wt %
AL 3-1	14.38
AL 3-2	17.14
AL 2-1	18.15
AL 2-1	18.02
AL 4-1	18.20
AL 4-2	17.70
AL 5-1	14.46
AL 5-2	13.51
AL 1-1	14.36
AL 1-2	14.56
UN 5-1	13.82
UN 5-2	14.14
UN 4-1	13.53
UN 4-2	14.07
UN 3-1	13.53
UN 3-2	13.63
UN 3-3	13.62
UN 3-4	13.38
UN 2-1	13.26
UN 2-2	16.35
UN 1-1	13.69
UN 1-2	11.13
AL (average)	16.05
UN (average)	13.68

Analyzing points	V (in Omp) ppm	V (in Rt) ppm	V ratio Rt/Omp
In2	475	2029	9 4.3
In2b	LOQ	N/A	N/A
In2c	491	2035	5 4.1
In5	LOQ	N/A	N/A
M1	352	1556	5 4.4
M2	353	1535	5 4.4
M3	341	1525	4.5
M5	351	1483	3 4.2
M6	496	1472	1 3.0

Table 4. LA-ICP-MS Vanadium concentration in omphacite and rutile between two phases.

Any LA-ICP-MS analyses below the limit of quantification (LOQ) or that show evidence of contamination by other phases (i.e., $\mathrm{Si} > 300$ ppm in rutile) were excluded, and the result were listed in Table 4. Vanadium concentrations are higher in rutile inclusions (> 2000 ppm) than in the matrix (~1500 ppm). However, matrix and inclusion omphacite are not distinguishable based on V concentration, and calculated V ratio based on this data also are not distinguishable within propagated uncertainty (Figures 8 and 9).

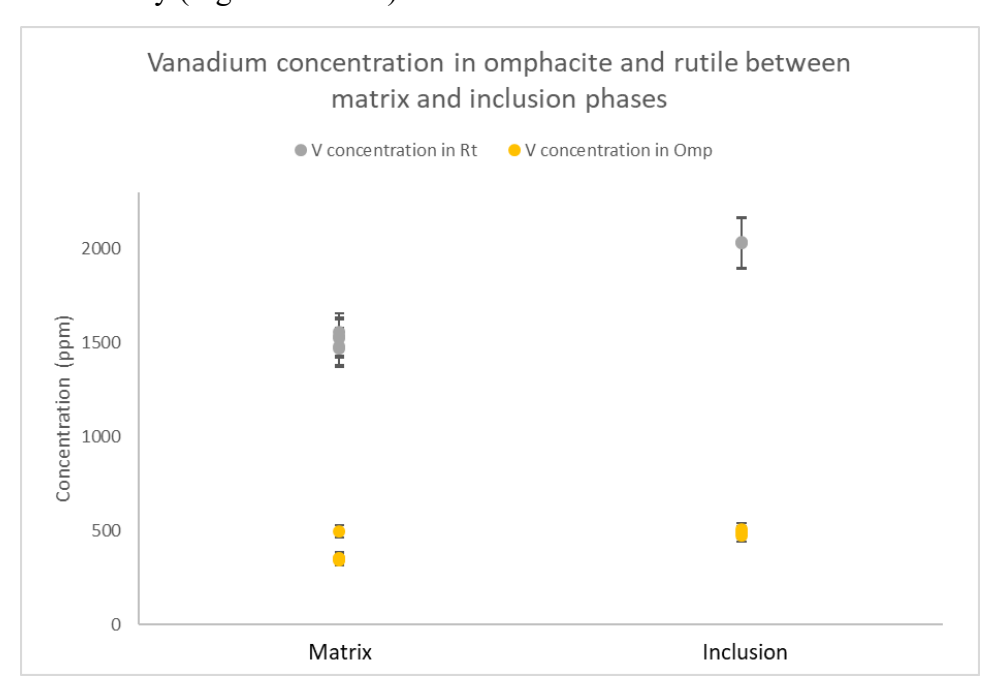


Figure 8. Vanadium concentration in rutile and omphacite in matrix and inclusion phases.

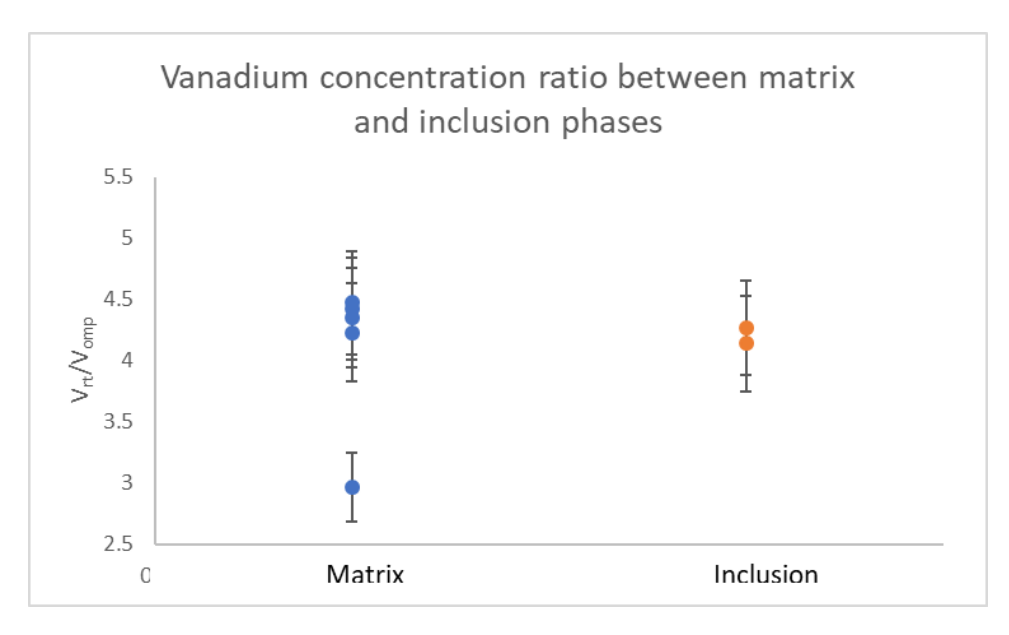


Figure 9. The V concentration ratio of rutile and omphacite in the matrix and the inclusion phases.

LA-ICP-MS result of the Monviso eclogite sample

Table 4 LA-ICP-MS analyzed the same locations aside from one rutile gran (4-1) which contains an inclusion that can impact the measuring accuracy.

Testing points (unaltered)	V in Omp (ppm)	V in Rt (ppm)
Un 1-1	620	1844
Un 1-2	732	1797
Un 2-1	749	1980
Un 2-2	890	2084
Un 4-1	605	N/A
Un 4-2	624	2307
Un 5-1	667	2379
Un 5-2	672	2404
Testing points (altered)	V in Omp (ppm)	V in Rt (ppm)
AL 1-2	730	1299
AL 2-1	524	1081
AL 2-2	290	1083
AL 3-1	600	1049
AL 3-2	657	1085
AL 4-1	712	984
AL 5-2	124	1033

A total of twenty-two omphacite and twenty rutile grains were analyzed by LA-ICP-MS and excluded analyses described above. Rims were chosen for the locations of analyses as they are thought to record the latest chemical equilibrium. Results acquired from both instruments,

with uncertainties, are calibrated, calculated, and listed in the Appendix. Internal standard calibrated and anomaly excluded LA-ICP-MS data are plotted in Figure 10.

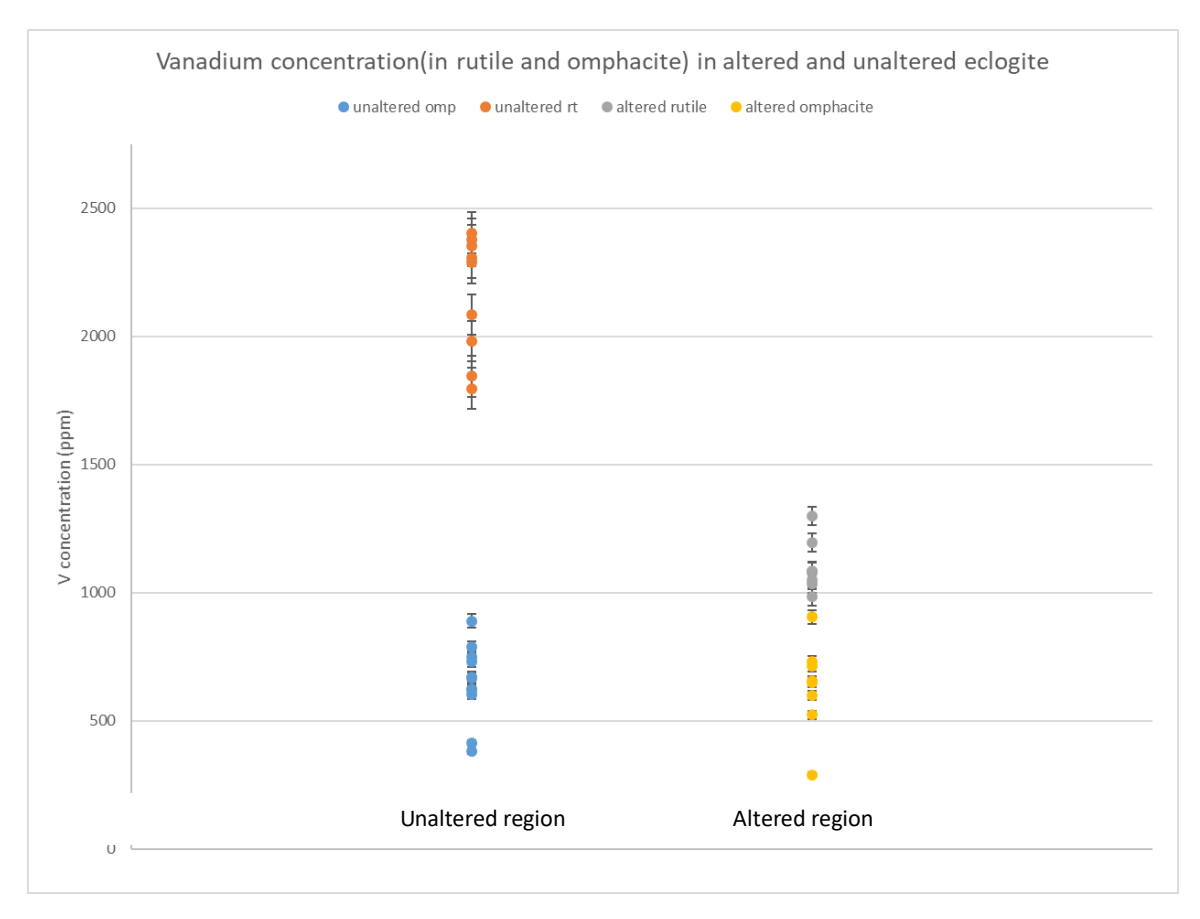


Figure 10. Vanadium concentration in Rt and Omp in altered and unaltered eclogite.

Because some omphacite grains are heterogeneous and have a variety of V concentrations (e.g., 524±15 and 290±9 ppm in unaltered omphacite No.2), the V concentration ratio is plotted in each pair with ranges in Figure 11. For grains with multiple analyses, a range of ratios is shown. To ensure all V ratio of each mineral pair between two regions is covered, the maximum value of each ratio is obtained by dividing the highest V concentration value in the rutile of that pair by the lowest V concentration value in omphacite and doing the opposite way to obtain the minimum value of each ratio.

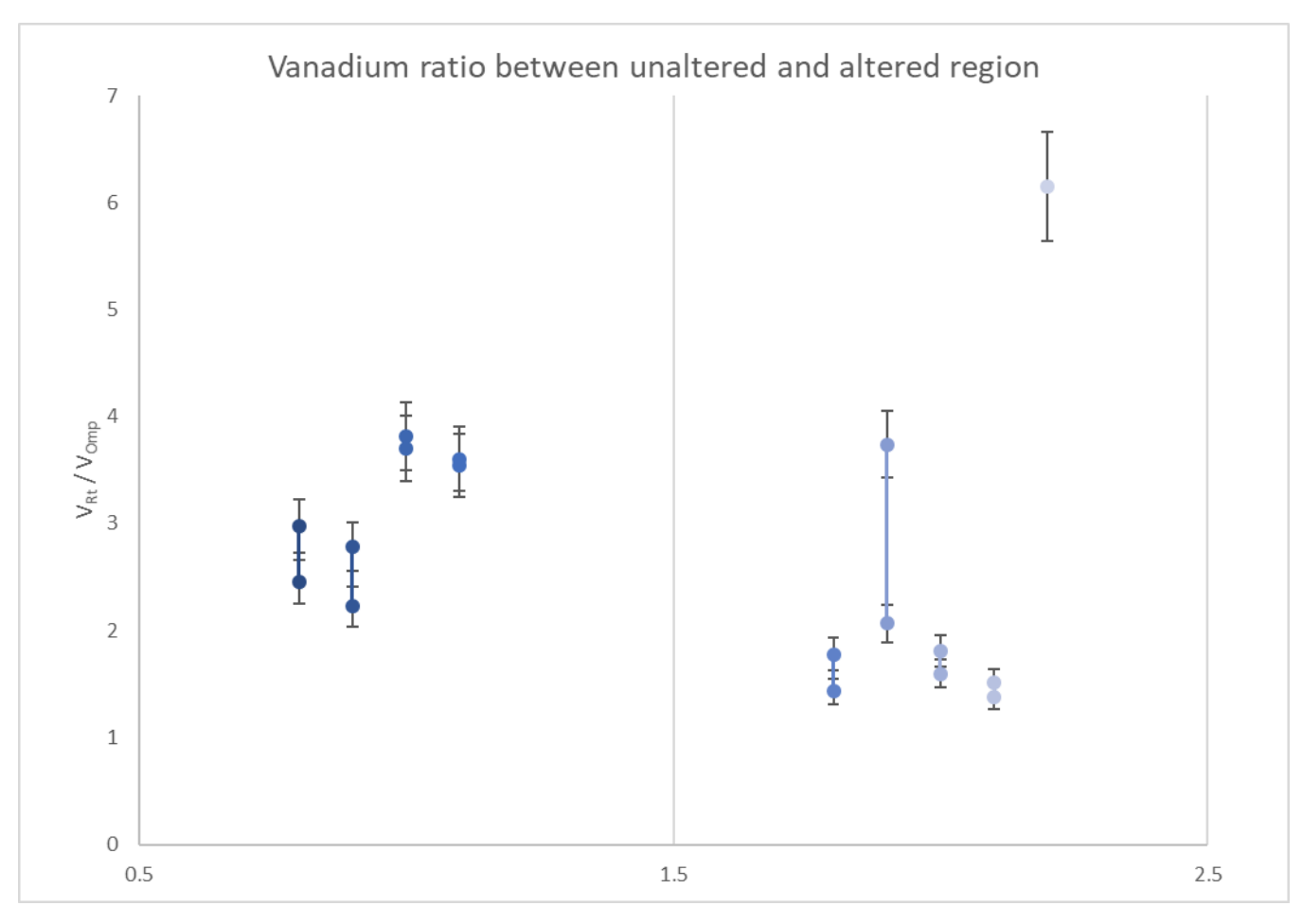


Figure 11. Vanadium concentration ratio range of Rt and Omp in two regions of Monviso sample.

Temperature result of two eclogite samples

Using Equation 2 from Tomkins et al. (2007), temperatures were estimated at 1.5 GPa for the Franciscan Complex and 2.6 GPa for the Monviso Complex based on the prior studies (Krogh et al., 1994; Angiboust et al., 2014). Calculated temperatures of each phase(region) of two samples overlapped. The Franciscan sample has temperature ranges from the inclusion phase between ~540°C and ~560°C, to the matrix phase from ~530°C to 580°C (Figure 12). The Monviso sample has more extensive temperature ranges than the Franciscan sample, with ~520°C to ~575°C in the unaltered region, and ~530°C to ~620°C in the altered region (Figure 13). However, the estimated average temperatures for two phases (regions) in two samples suggest phases and regions formed in similar temperature conditions, and they are close to the peak metamorphic conditions reported for each location, with 560°C for the Franciscan Complex and 550°C for the Monviso Metaophiolite Complex (Krogh et al., 1994; Angiboust et al., 2011). Also, the temperature estimation of the Monviso Metaophiolite Complex sample suggested that the alteration event took place under eclogite facies, in agreement with the estimated metasomatism condition by Angiboust et al. (2011).

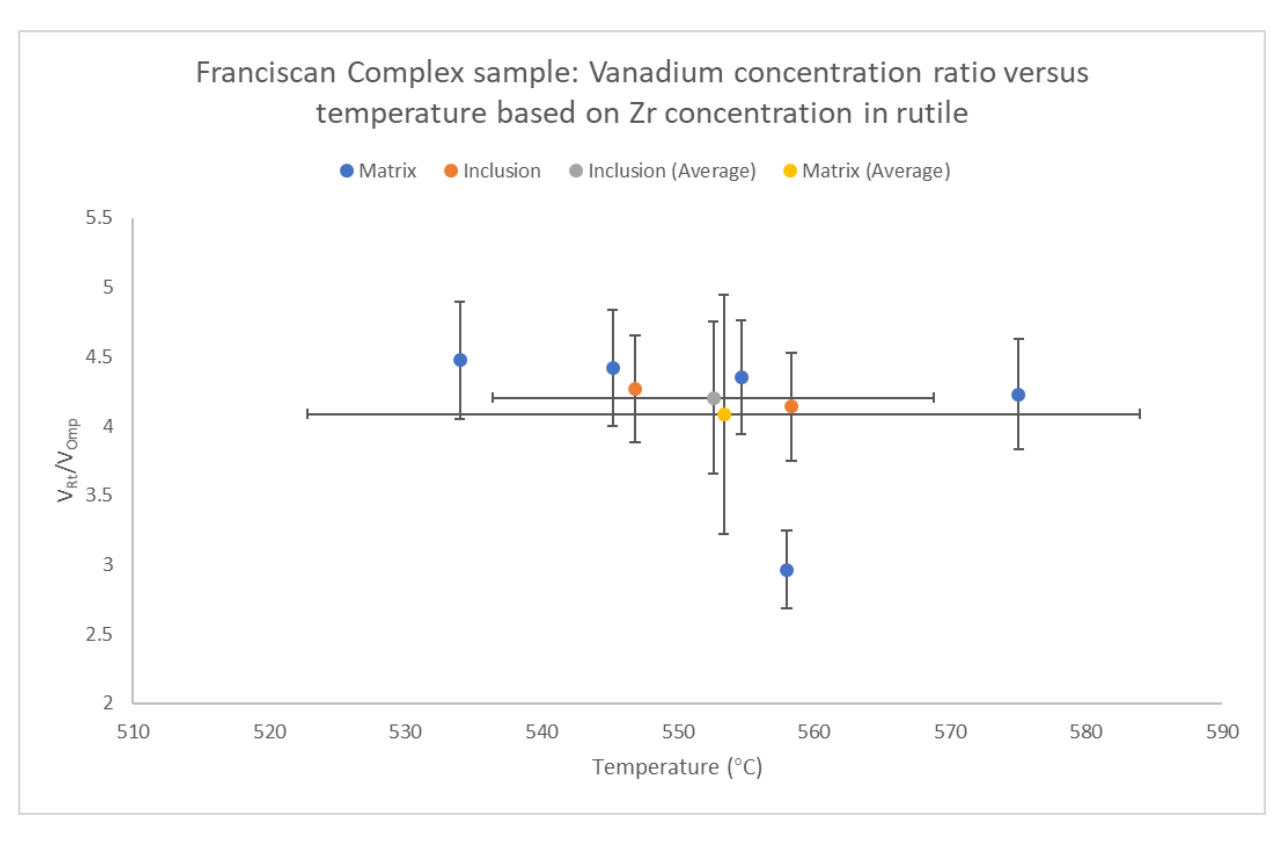


Figure 12. Vanadium concentration ratio versus temperature for the Franciscan Complex sample. Temperatures were estimated at 1.5 GPa. Two standard deviations were only applied on estimated average temperatures and for two regions.

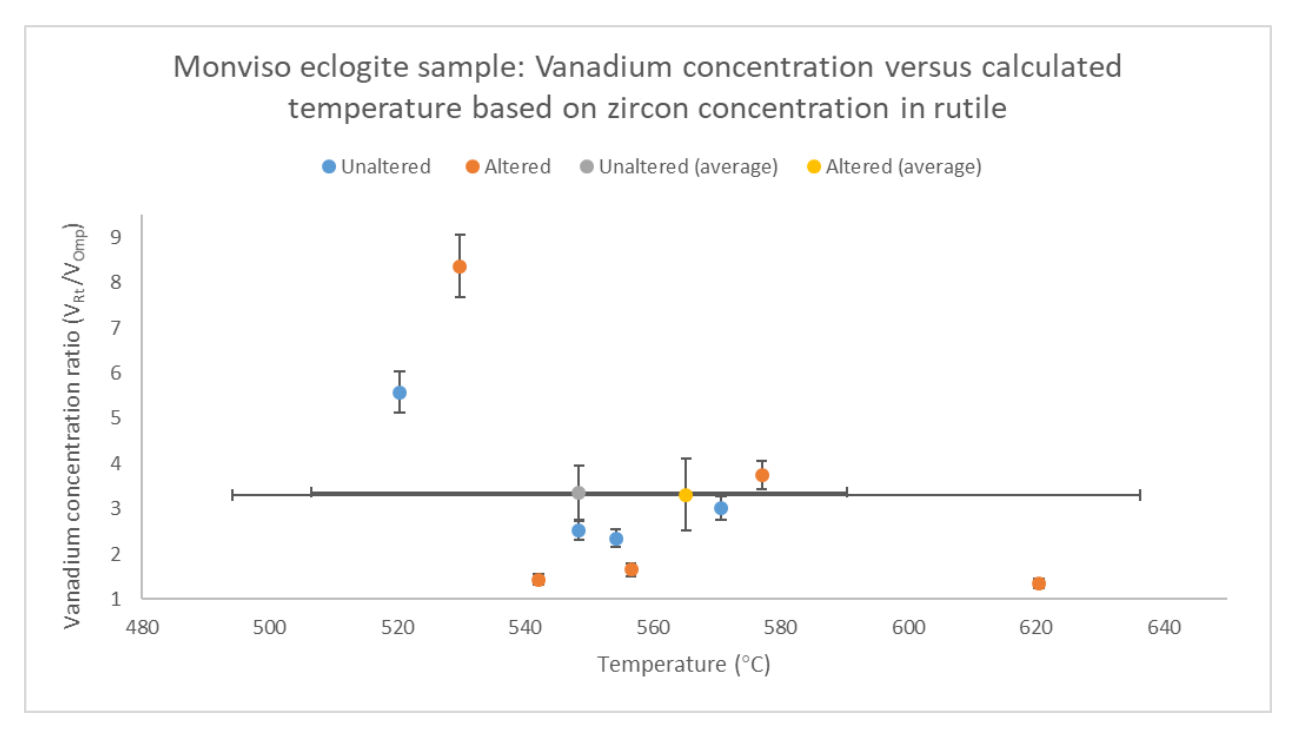


Figure 13. Vanadium concentration ratio versus temperature for the Monviso Complex sample. Temperatures were estimated at 2.6 GPa. Two standard deviations were only applied on estimated average temperatures and for two regions.

Discussion

Vanadium ratio recorded in rocks reflects oxygen fugacity, however it can be changed by different mechanisms such as pressure, temperature, and chemical environment (Holycross and Cottrell, 2020). Therefore, this section will discuss each mechanism and its impact on V partitioning based on data obtained from two samples.

Changes in V partitioning as a result of prograde metamorphism.

Although the V concentration of rutile is lower in the matrix phase with one outlier in which the rutile is surrounded by alteration mineral titanite (Figure 24 in Appendix), the V concentration ratio (Figure 9) of the Franciscan Complex sample is not different between matrix phases and inclusions in garnet. This result suggests either that oxygen fugacity did not change during eclogite-facies metamorphism or that the inclusions and matrix phases are recording the same metamorphic event. The presence of glaucophane as both retrograde and prograde minerals that deposited along with garnet fractures and inside omphacite as an inclusion, respectively (Figure 14), suggest oxygen fugacity recorded on the mineral edges may have changed before and after both matrix and inclusion phases crystallized and resulted in a similar V concentration ratio between two metamorphic stages. The metamorphic pathway (Krogh et al., 1994) suggested the blueschist facies metamorphic rock that enriched in hydrous minerals such as glaucophane. progressively dehydrated, and it transferred oxidation potential into the mantle as P-T conditions increased. Prograde metamorphic dehydration reactions could have occurred before omphacite was stable in this rock and transferred oxidation potential from the slab to surroundings, as described in Kelley and Cottrell (2009). The reappearance of glaucophane as a retrograde mineral may indicates this rock had rehydrated as the P-T conditions decreased after the peak condition. The Franciscan samples show distinct V partitioning differences in rutile between two phases. However, estimated temperatures that based on Zr in rutile for different phases overlap, which indicates temperature was not the changing mechanism for V ratio in this sample.

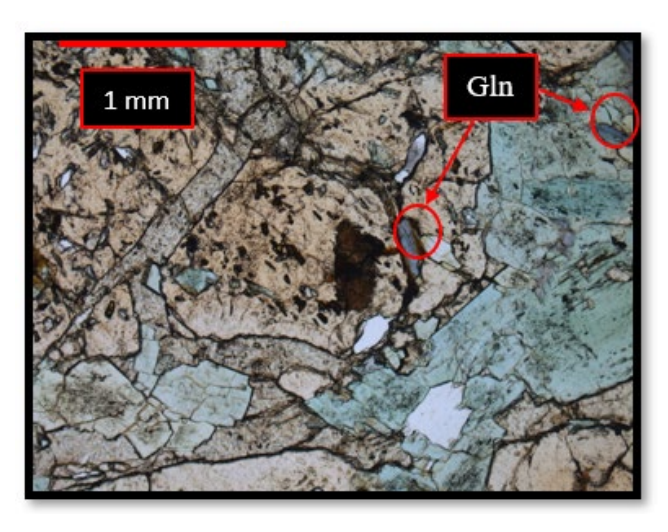


Figure 14. glaucophane (Gln) deposited along with garnet fractures and as inclusion.

Changes in V partitioning as a result of metasomatism

Vanadium concentrations of rutile in the altered region of the Monviso thin section are distinctly different from the V concentrations of rutile in the unaltered region that it shows a clear and distinct difference. This indicates that rutile in the two regions were formed in different chemical environments, such as different temperature, oxygen fugacity, or bulk-rock V concentration. However, temperature overlaps shown in Figure 13 indicate the V ratio variations represented between the two regions are not the results of differences in temperature between the unaltered rock and the metasomatism. Therefore, different oxygen fugacity and/or chemical compositions are seeming to be responsible for chemically different rutile. In contrast to rutile, the V concentrations of omphacite from the two regions of the thin section overlap, with a higher range of V concentrations in the altered region.

In the majority of the samples, the unaltered eclogite records a higher V ratio. This reflects the higher overall V concentration of rutile. Two outliers that caused by small V concentrations in omphacite show significant ratio values that do not make consistent with other ratios: one outlier has a ratio range overlap both population and another one has a V ratio which about three times larger than the rest ratios in the altered region (Figure 11).

The textural relationship at these analysis spots may explain the variations in V concentration. Sector zoning within omphacite grains, other chemical zonings, and analytical problems such as hitting cracks, could have caused the observed variations. Therefore, by comparing the shape and other textures of the omphacite grains, and locations of analyses on them in PPL and RL images, the various V concentration in three mineral pairs are likely to be interpreted as; 1) pair No.2 (Figure 15) in the altered region, contributed non-uniform element distribution. 2) New chemical equilibrium contributed new large-sized omphacite grains with elongated shapes such as the analyzed omphacite of pair No.5 (Figure 16) in the altered region and deposited a new chemical composition with slightly different major elements. Vanadium ratio in Figure 11 decreased from the unaltered to altered regions supports the second hypothesis that the rock-fluid interaction would cause changes in the V concentration ratio of rutile and omphacite from unaltered to altered regions.

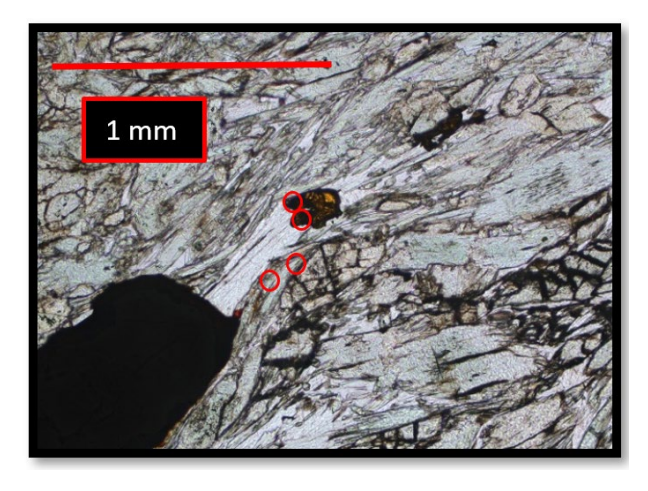


Figure 15. The altered mineral pair No.2 of the Monviso Metaophiolite Complex sample. Two analysis spots on each mineral rim are marked in red circles.

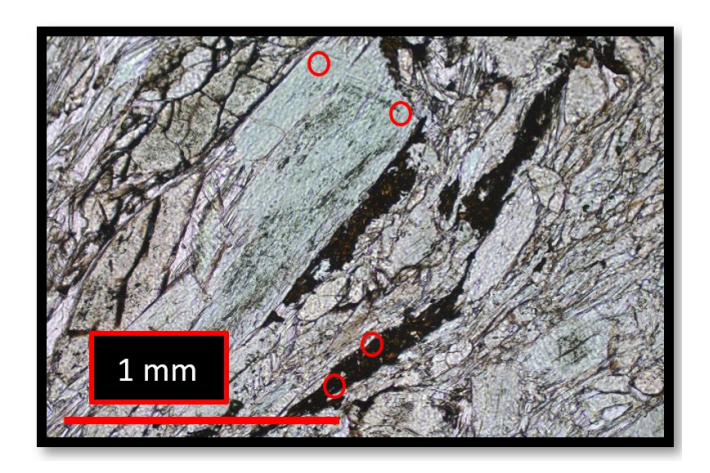


Figure 16. The altered mineral pair No.5 of the Monviso Metaophiolite Complex sample. Two analysis spots on each mineral rim are marked in red circles.

Changes in V partitioning as a result of new chemical equilibrium

Observed major element differences between the altered and unaltered regions suggest there could had a significant change in the bulk composition to the rock, and impact trace element partitioning. A change in one major element of omphacite will affect other major elements that sit in the same structural site, such as Al concentrations, which corresponded to V^{3+} partitioning that fits the same mineral structural site. Therefore, the aluminum oxide (Al₂O₃) concentration data, were compared to V concentration data (Figure 17) to see if there were any systematic variations between Al and V. While altered omphacite has lower Al₂O₃ on average with 4.11 ± 0.260 wt%, Al₂O₃ compositions overlap and there is no clear evidence that V content correlates with Al₂O₃ or any other major element such as Fe and Mg.

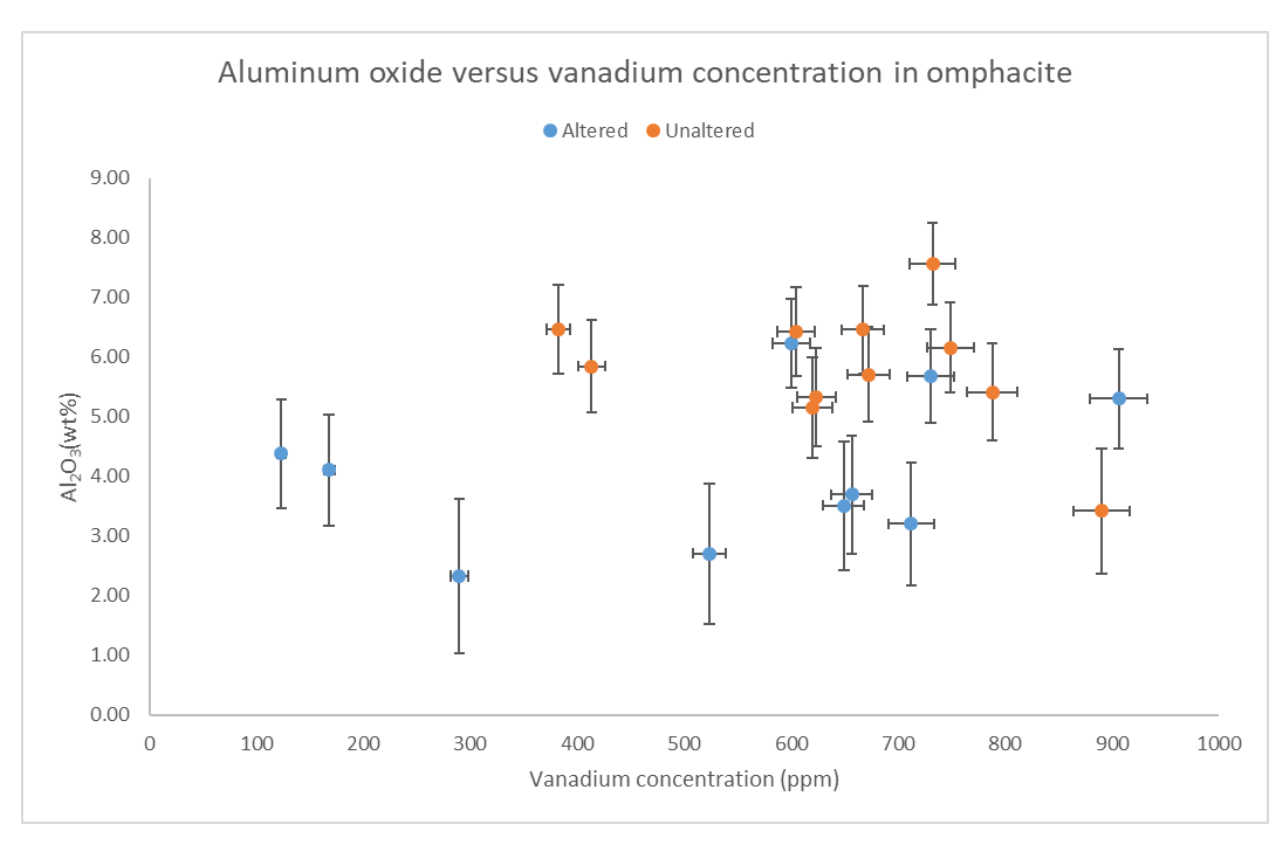


Figure 17. Aluminum oxide data of each region collected by EPMA versus V concentration data of two regions collected by LA-ICP-MS.

Vanadium concentration in rutile and omphacite of the Monviso sample is similar to the result obtained from the Franciscan Complex eclogite sample (Figures 10 and 8), with mostly decoupled V concentration ranges in rutile, and heavily overlapped V concentration ranges in omphacite between matrix and inclusion phases. Although V concentrations are similar in two regions between two samples, it is hard to draw any comparison because the starting composition of each rock is unknown.

Conclusion and implication

Apparent differences exist in V contents of rutile in both the Franciscan Complex and Monviso Metaophiolite Complex samples. However, the Franciscan Complex eclogite sample did not show any significant V concentration ratio difference between the matrix and the inclusion phases. It supports the first null hypothesis and elicited one possible explanation to this result is that oxygen fugacity had changed before and after both phases crystallized and impacted V partitioning. The result of an altered Monviso eclogite supports the second hypothesis with a decreasing V concentration ratio from unaltered to altered regions. Temperatures estimated based on recorded Zr contents in rutile of two samples overlap between two regions(phases), indicating temperature did not affect the V partitioning in these rocks. Also, no correlations between major element concentrations and V partitionings have shown in both Monviso and Franciscan samples. Therefore, by excluding change in temperature and change in chemical compositions, the only option that provides variation is the fluid, either catalyzed or escaped as a product of the

metasomatism or metamorphism, had a different oxygen fugacity than the block. This study implies that changes in oxygen fugacity represented by V partitioning in minerals occur during subduction and are associated with fluid that supports the findings of Kelley and Cottrell (2009).

Acknowledgements

I would like to gratefully acknowledge Dr. Sarah Penniston-Dorland for her expertise and Godgiven patience that carefully guided me through the thesis process. I would like to thank Dr. Philip M. Piccoli and Dr. Richard Ash for utilizing the EPMA and LA-ICP-MS in their lab rooms, answering my numerous questions, and providing brilliant solutions to the problems that I could not solve. I would like to thank Dr. Sarah Penniston-Dorland, Will Hoover, Kayleigh Harvey, Christiana Hoff, Sona Chaudhary, and Cristy Ho for their very provocative, constructive advice on this project.

BIBLIOGRAPHY

- Aulbach, S., & Stagno, V. (2016). Evidence for a reducing Archean ambient mantle and its effects on the carbon cycle. Geology, 44(9), 751–754. doi: 10.1130/g38070.1
- Angiboust, S., Langdon, R., Agard, P., Waters, D., & Chopin, C. (2011). Eclogitization of the Monviso ophiolite (W. Alps) and implications on subduction dynamics. *Journal of Metamorphic Geology*, *30*(1), 37–61. doi: 10.1111/j.1525-1314.2011.00951.x
- Angiboust, S., Pettke, T., Hoog, J. C. M. D., Caron, B., & Oncken, O. (2014). Channelized Fluid Flow and Eclogite-facies Metasomatism along the Subduction Shear Zone. *Journal of Petrology*, *55*(5), 883–916. doi: 10.1093/petrology/egu010
- Catlos, E. J. (2003). Phengite-Based Chronology of K- and Ba-Rich Fluid Flow in Two Paleosubduction Zones. *Science*, *299*(5603), 92–95. doi: 10.1126/science.1076977
- Frost, B. R. (1991, January 1). Introduction to oxygen fugacity and its petrologic importance. Retrieved from https://pubs.geoscienceworld.org/msa/rimg/article-abstract/25/1/1/87287/introduction-to-oxygen-fugacity-and-its-petrologic.
- Holycross, M., & Cottrell, E. (2020). Partitioning of V and 19 other trace elements between rutile and silicate melt as a function of oxygen fugacity and melt composition: Implications for subduction zones. *American Mineralogist*, 105(2), 244–254. doi: 10.2138/am-2020-7013
- Kelley, K. A., & Cottrell, E. (2009). Water and the Oxidation State of Subduction Zone Magmas. *Science*, *325*(5940), 605–607. doi: 10.1126/science.1174156
- Kelley, K. A., & Cottrell, E. (2012). The influence of magmatic differentiation on the oxidation state of Fe in a basaltic arc magma. *Earth and Planetary Science Letters*, *329-330*, 109–121. doi: 10.1016/j.epsl.2012.02.010
- Krogh, E. J., Oh, C. W., & Liou, J. C. (1994). Polyphase and anticlockwise P-T evolution for Franciscan eclogites and blueschists from Jenner, California, USA. *Journal of Metamorphic Geology*, *12*(2), 121–134. doi: 10.1111/j.1525-1314.1994.tb00008.x
- Liu, L., Xiao, Y., Aulbach, S., Li, D., & Hou, Z. (2014). Vanadium and niobium behavior in rutile as a function of oxygen fugacity: evidence from natural samples. *Contributions to Mineralogy and Petrology*, *167*(6), 1–22. doi: 10.1007/s00410-014-1026-2
- Locatelli, M., Federico, L., Agard, P., & Verlaguet, A. (2019). Geology of the southern Monviso metaophiolite complex (W-Alps, Italy). *Journal of Maps*, *15*(2), 283–297. doi: 10.1080/17445647.2019.1592030
- Luvizotto, G., Zack, T., Meyer, H., Ludwig, T., Triebold, S., Kronz, A., ... Eynatten, H. V. (2009). Rutile crystals as potential trace element and isotope mineral standards for microanalysis. *Chemical Geology*, 261(3-4), 346–369. doi: 10.1016/j.chemgeo.2008.04.012

- Mengason, M., & Ritchie, N. (2017). Overcoming Peak Overlaps in Titanium- and Vanadium-Bearing Materials with Multiple Linear Least Squares Fitting. *Microscopy and Microanalysis*, 23(3), 491–500. doi: 10.1017/s1431927617000265
- Tollan, P., & Hermann, J. (2019). Arc magmas oxidized by water dissociation and hydrogen incorporation in orthopyroxene. *Nature Geoscience*, *12*(8), 667–671. doi: 10.1038/s41561-019-0411-x
- Tomkins, H. S., Powell, R., & Ellis, D. J. (2007, July 21). The pressure dependence of the zirconium-in-rutile thermometer. Retrieved from https://onlinelibrary.wiley.com/doi/full/10.1111/j.1525-1314.2007.00724.x
- Whitney, D. L., & Evans, B. W. (2010). Abbreviations for names of rock-forming minerals. *American Mineralogist*, *95*(1), 185–187. doi: 10.2138/am.2010.3371
- Xiong, X., Adam, J., & Green, T. (2005). Rutile stability and rutile/melt HFSE partitioning during partial melting of hydrous basalt: Implications for TTG genesis. Chemical Geology, 218(3-4), 339–359. doi: 10.1016/j.chemgeo.2005.01.014
- Zack, T., & Kooijman, E. (2017). Petrology and Geochronology of Rutile. *Reviews in Mineralogy and Geochemistry*, 83(1), 443–467. doi: 10.2138/rmg.2017.83.14
- Zack, T., Moraes, R., & Kronz, A. (2004). Temperature dependence of Zr in rutile: empirical calibration of a rutile thermometer. *Contributions to Mineralogy and Petrology, 148*(4), 471–488. doi: 10.1007/s00410-004-0617-8
- Zhao, D., Essene, E. J., & Zhang, Y. (1999). An oxygen barometer for rutile—ilmenite assemblages: oxidation state of metasomatic agents in the mantle. *Earth and Planetary Science Letters*, *166*(3-4), 127–137. doi: 10.1016/s0012-821x(98)00281-7

Appendices

Appendix 1. Thin section scan $(4.6 \times 2.7 \text{ cm})$ of the Franciscan sample. Matrix and inclusion pairs are circled in red with labels "M" and "In". PPL light images of all sites are oriented closely along with the thin section.

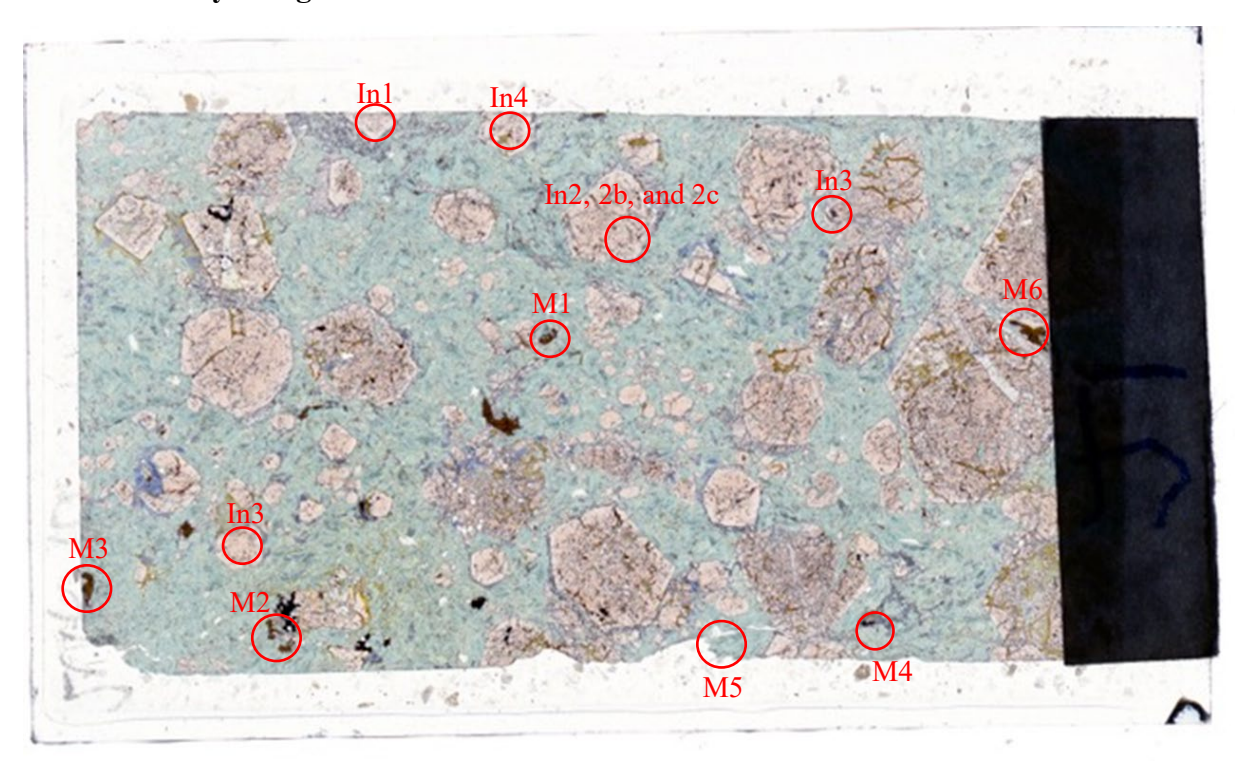


Figure 18. Thin section of the Franciscan sample.

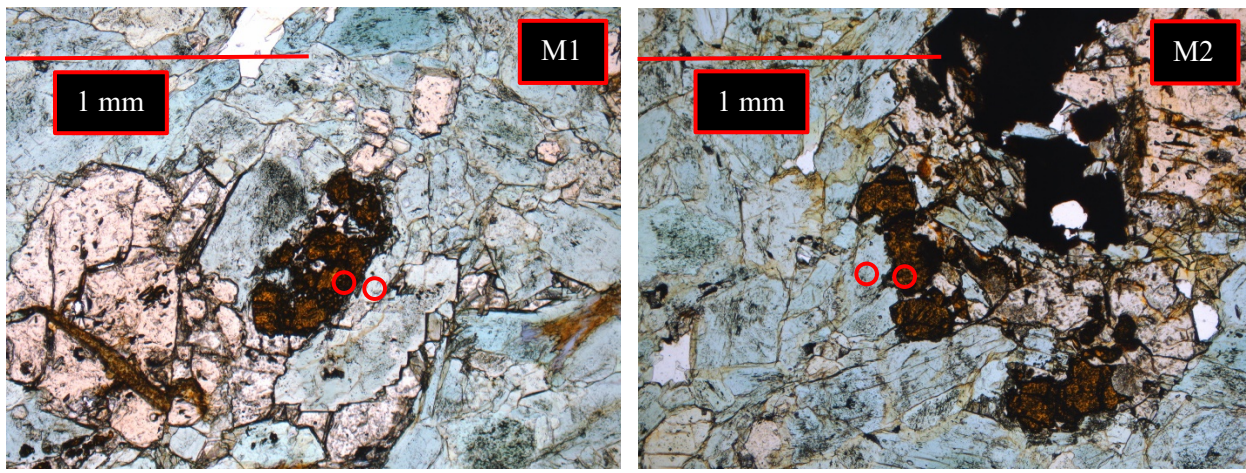


Figure 19. M1 under PPL. Objective: 5x.

Figure 20. M2 under PPL. Objective: 5x.

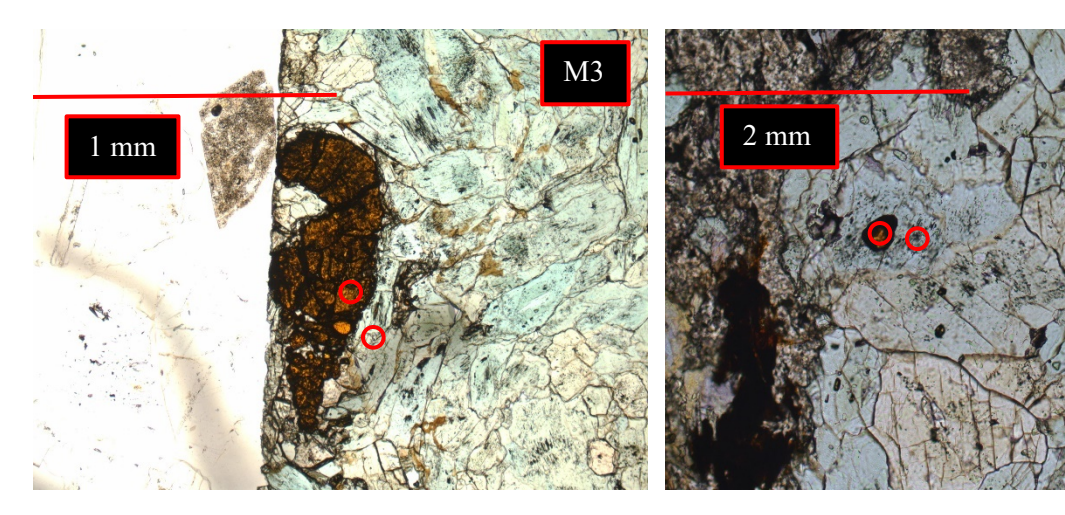


Figure 21. M3 under PPL. Objective: 5x.

Figure 22. M4 under PPL. Objective: 10x.

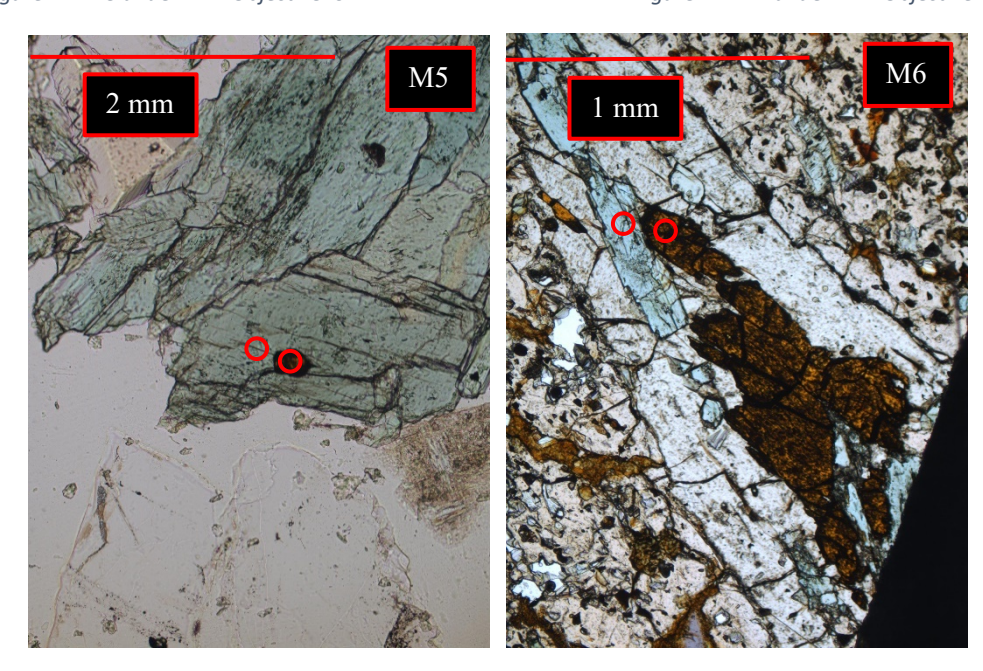


Figure 23. M5 under PPL. Objective: 10x.

Figure 24. M6 under PPL. Objective: 5x.

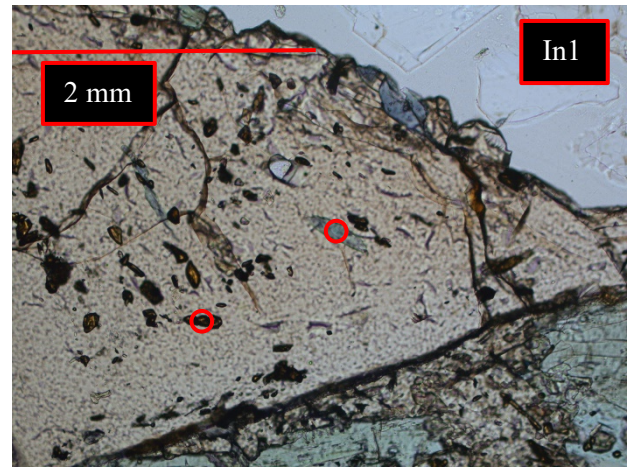


Figure 25. In1 under PPL. Objective: 10x.

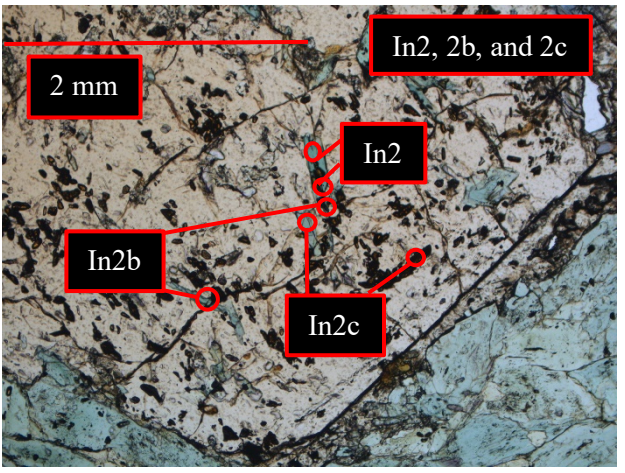


Figure 26. In2, In2b, and In2c under PPL. Objective: 10x.

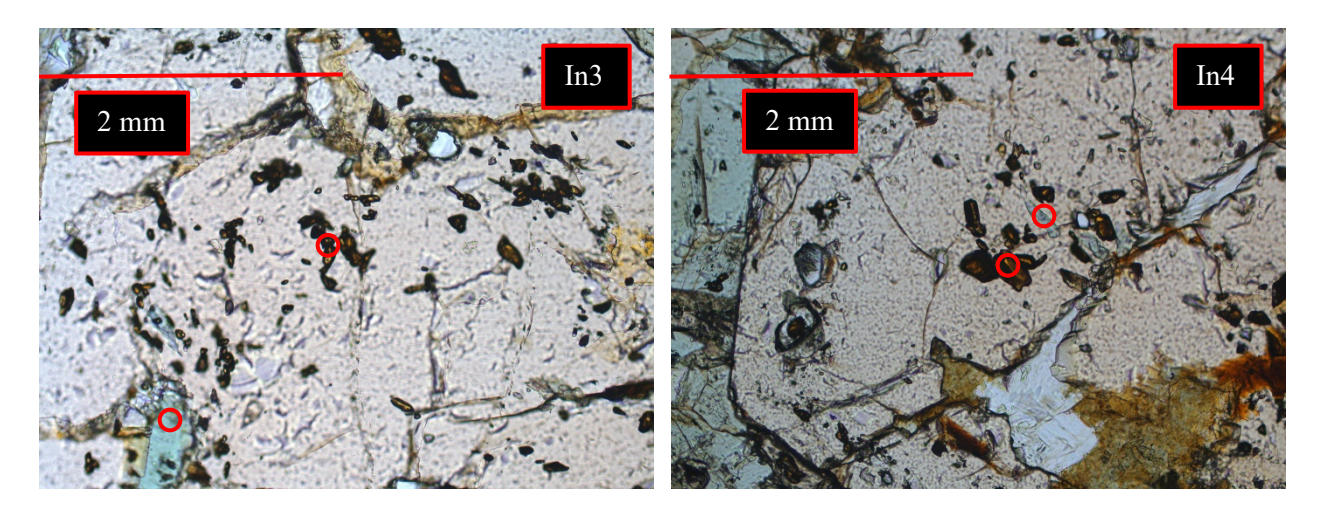


Figure 27. In 3 under PPL. Objective: 10x.

Figure 28. In4 under PPL. Objective: 10x.

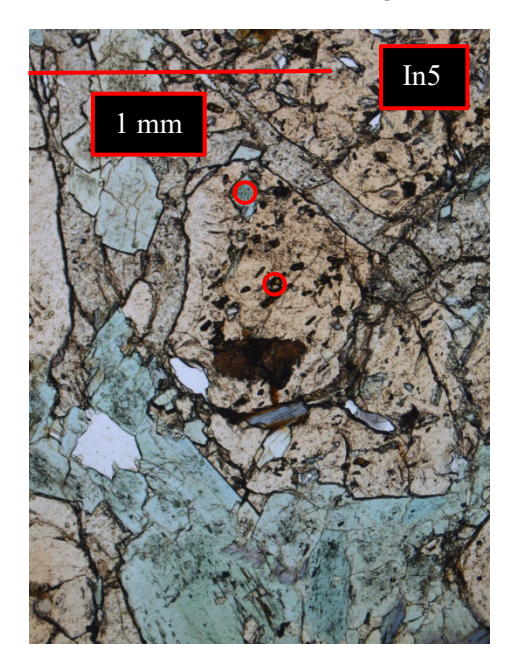


Figure 29. In5 under PPL. Objective: 5x.

Appendix 2. Thin section scan (4.6 x 2.7 cm) of the Monviso sample. UN 1

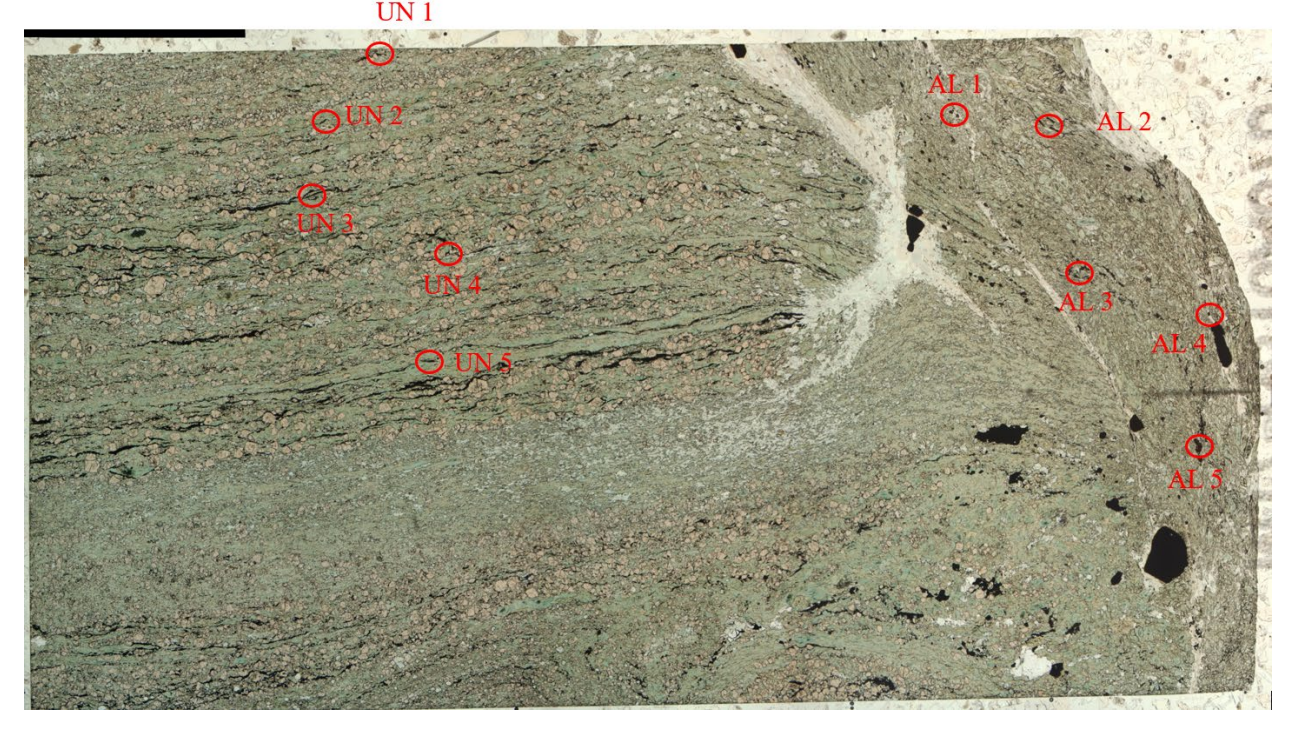


Figure 30. Thin section of the Monviso sample

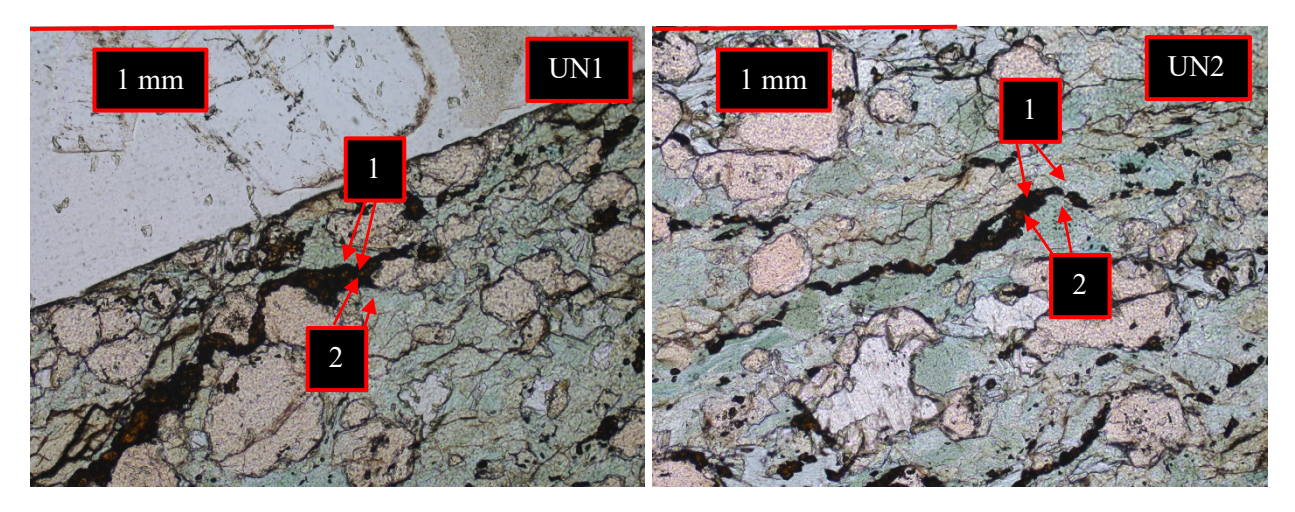


Figure 31. UN1 under PPL. Objective: 10x.

Figure 32. UN2 under PPL. Objective: 10x.

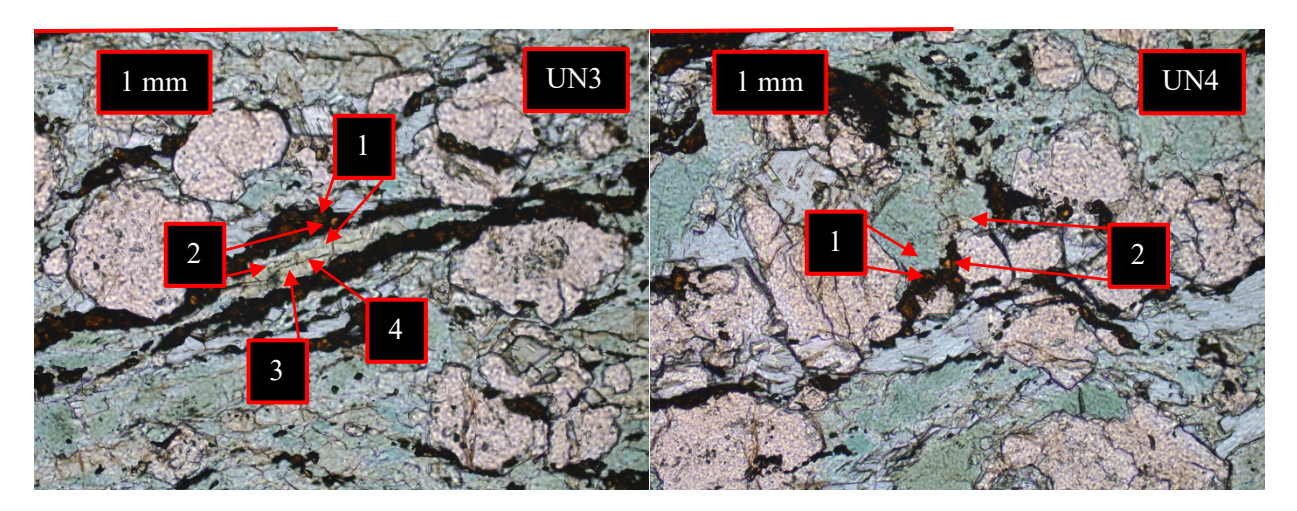


Figure 33. UN3 under PPL, 4analyses on omphacite Objective: 10x. Figure 34. UN4 under PPL. Objective: 10x.

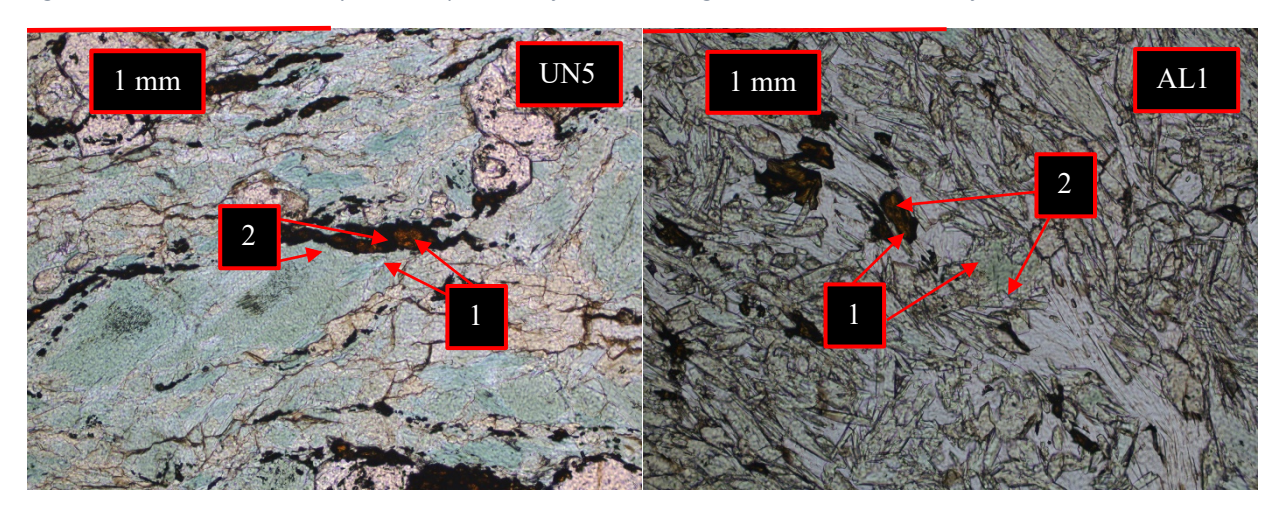


Figure 35. UN5 under PPL. Objective: 10x.

Figure 36. AL1 under PPL. Objective: 10x.

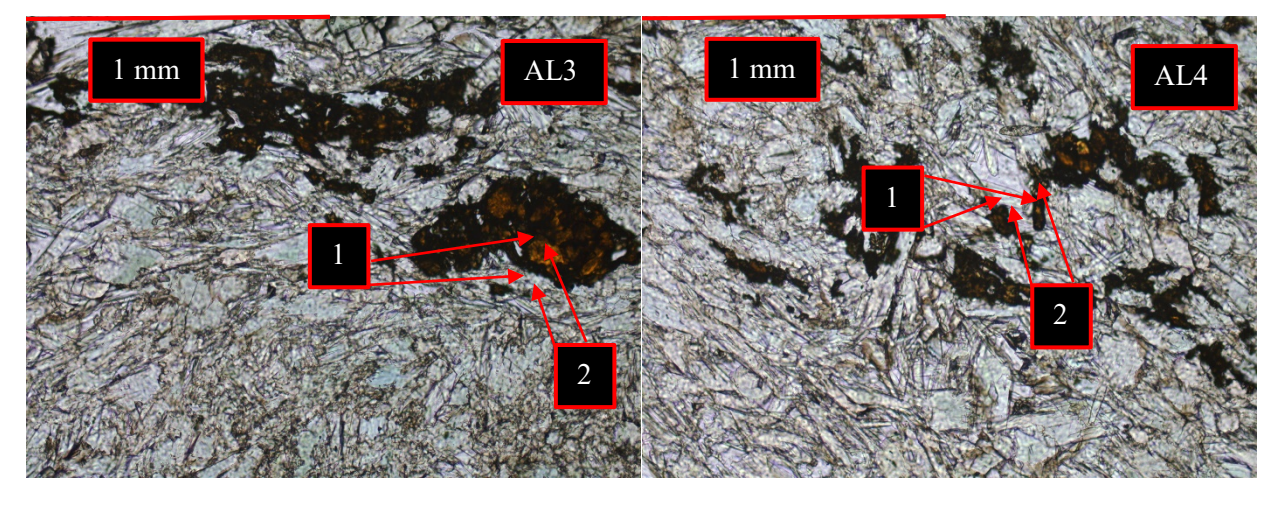


Figure 37. AL3 under PPL. Objective: 10x.

Figure 38. AL4 under PPL. Objective: 10x.

Appendix 3. Methods description: EPMA

The EPMA is a microbeam instrument that can acquire the composition of sample by exerting a non-destructive electronic beam. One EPMA has multiple detectors that function in different ways; thus, it can acquire comprehensive mineralogic information of the sample. Back-scattered electron (BSE) imaging will help differentiate the minerals composed of different elements on the thin section map. The EDS can generate a faster analysis than WDS of the EPMA, but WDS can provide a quantitative, precise composition data of a spot (1-2 micronsized) on the sample than the EDS.

During the experiment, a continuous beam of electrons was generated from the cathode, and it interacted with the sample by knocking out electrons from the inner shell. With an electron vacancy in the inner shell, an electron dropped down from the outer shell to create a stable configuration and emitted an X-ray during this process. Different elements have different characteristics of X-rays (wavelengths and energies). X-rays are focused using a bent crystal that leads the beams toward a detector. The computer collects and corrects the raw intensity into quantitative data by using ZAF (Z: atomic number, A: absorption, F: fluorescence) correction.

Vanadium concentrations are hard to determine due to the cascading overlaps of transition metals (Mengason & Ritchie, 2017). V K α overlaps with Ti K β , and V K β overlaps with Cr K α (Figure 39). Therefore, in this study, only V and other trace element concentrations collected by LA-ICP-MS will be used for results interpretations. However, EPMA analysis is still essential since major elements concentration data collected by EPMA are used as internal standards to calibrate the LA-ICP-MS data and thus are required for this work.

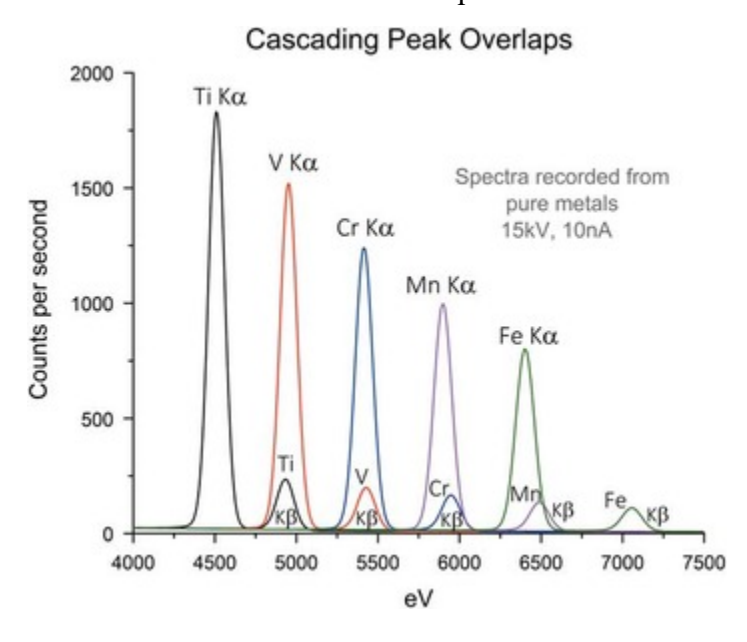
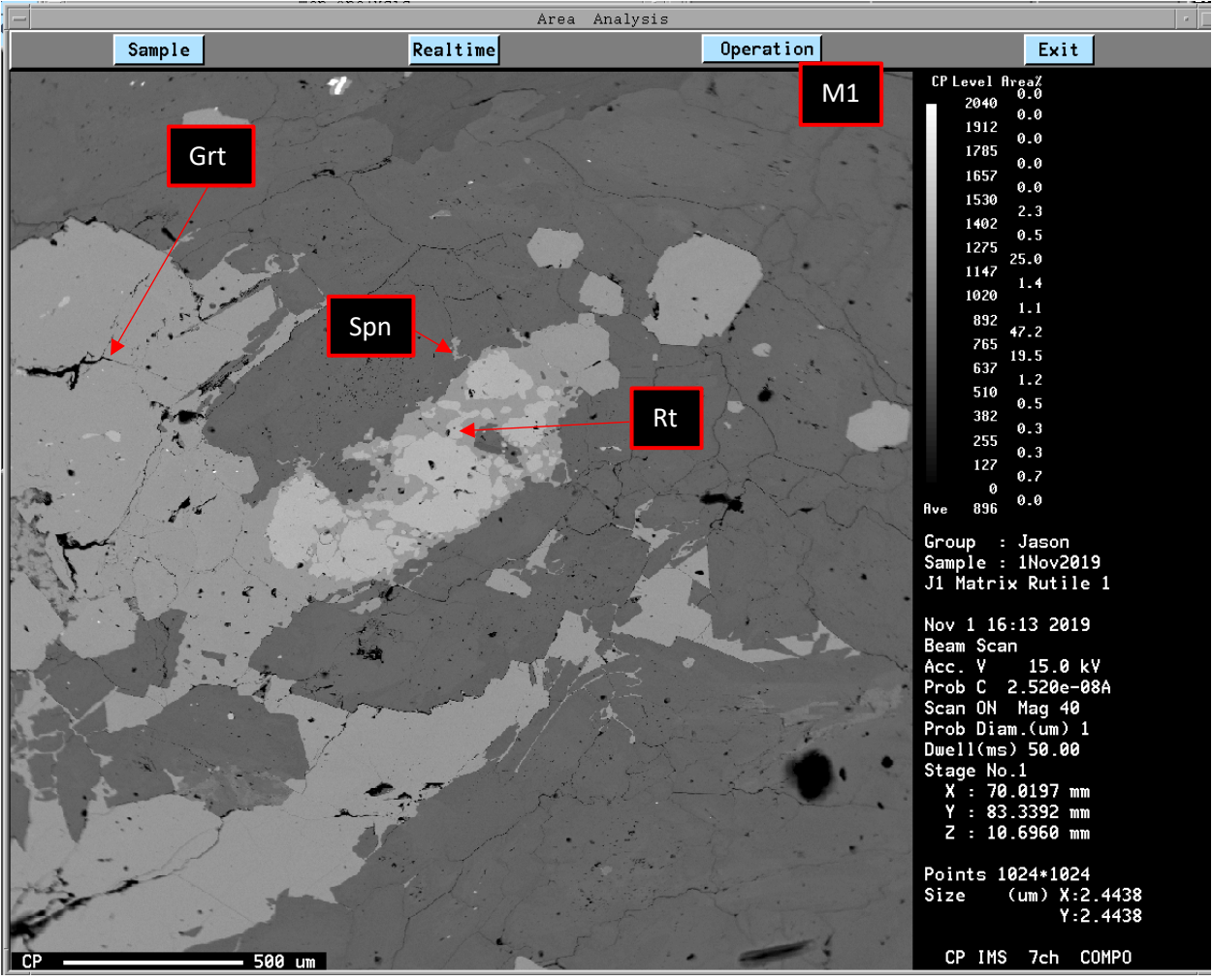


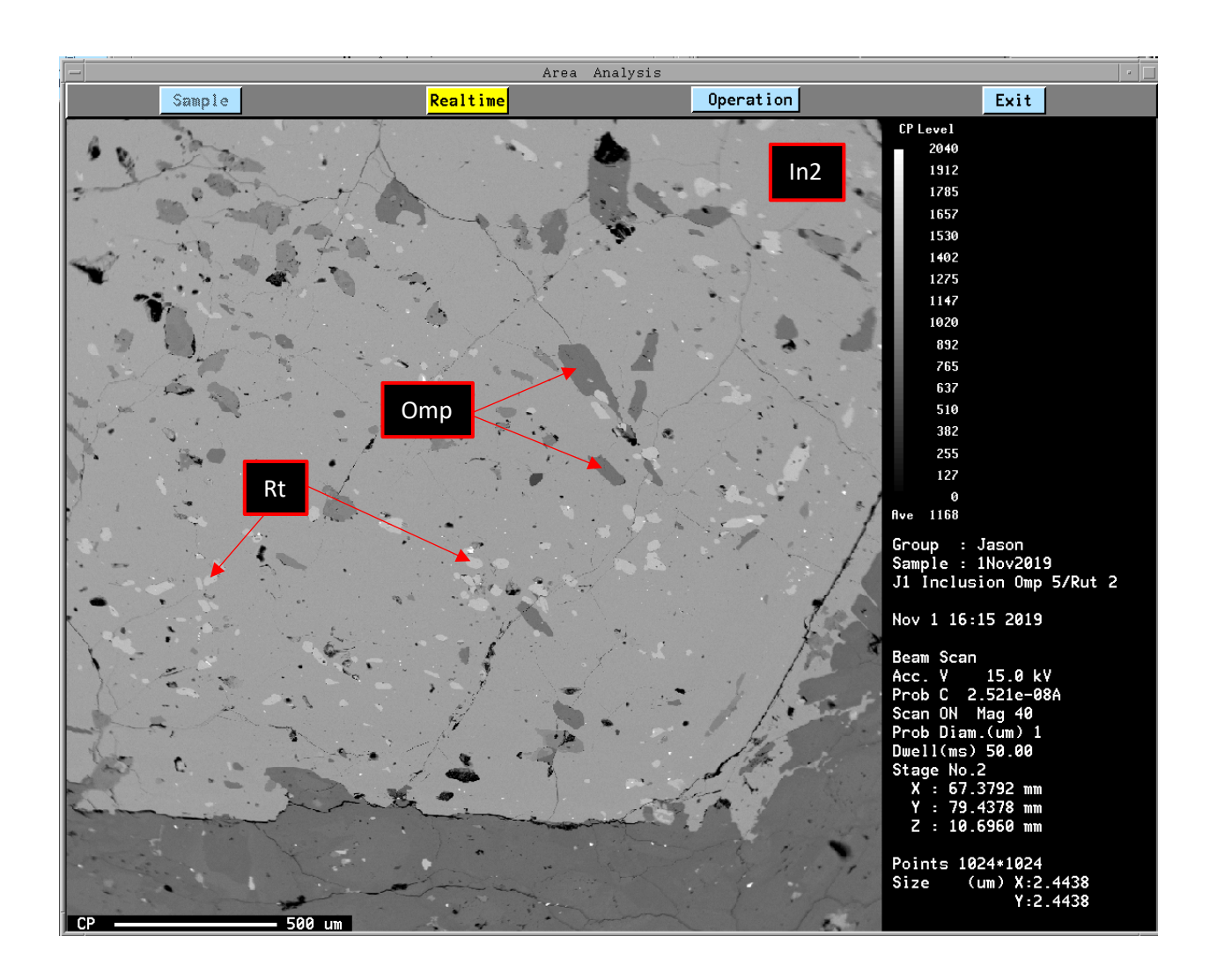
Figure 39. Cascading peak overlaps on transition metals (Mengason & Ritchie, 2017).

Appendix 4. Standard deviation of NIST610 calculated from eight analyses for two samples in one significant figure. * represents the RSD in three significant digits.

•	d NIST610 for the Fra Ionviso Complex eclogi	
NIST610	Vanadium (ppm)	
Analysis-1	428	446
Analysis -2	472	472
Analysis -3	464	460
Analysis -4	436	440
Analysis -5	440	444
Analysis -6	460	456
Analysis -7	454	450
Analysis -8	446	450
Average	450	450
Standard deviation	15	7
Franciscan Complex sa	ample RSD (%) = $(15/45)$	$50) \cdot 100 = 3 (3.34*)$
Monviso Complex sa	ample RSD (%) = $(7/450)$	1000 = 1(1.47*)

Appendix 5. Backscattered electron images on M1 and In2. Mineral boundaries are clearer by using backscattered electron images compared to plane polarized light images.





Appendix 6. Chemistry property data of the Franciscan sample obtained by EPMA.

EPMA result Omphacite Unit: wt%	Omphacite											
No.	Na20	FeO	Nb205	V203	AI2O3	MgO	MnO	K20	Ti02	Si02	CaO	Total
In1	6.743	11.853	-0.033	0.147	8.436	6.452	0.017	0.026	0.074	53.808	11.085	809.86
In2	6.927	12.011	-0.028	0.149	8.340	6.041	-0.001	0.008	090.0	53.922	10.944	98.372
In2b	6.926	12.701	0.044	0.178	8.621	5.844	0.015	0.034	0.093	53.920	10.765	99.141
In2c	7.089	12.134	0.068	0.154	8.766	5.989	0.017	0.026	0.064	53.978	10.707	98.991
In3	692.9	12.910	-0.022	0.130	8.026	2.767	0.034	0.023	0.057	54.045	10.460	98.200
In4	6.794	12.760	-0.006	0.177	7.974	6.024	0.070	0.024	0.090	53.886	10.738	98.531
In 5	6.484	11.182	0.074	0.203	8.691	6.002	0.022	0.024	0.061		11.562	98.359
M1	6.531	10.051	0.064	0.076	9.052	6.561	960.0	0.045	0.023	54.423	11.252	98.174
M2	5.893	8.323	0.034	0.088	8.545	8.247	0.031	0.020	0.078		13.413	99.449
M3	5.823	8.081	900.0	0.113	8.545	8.041	0.013	0.019	0.028		13.157	98.221
M4	6.254	8.690	-0.028	0.149	9.011	7.559	-0.004	0.013	0.117	54.620	12.411	98.791
M5	7.058	11.648	0.023	0.169	8.765	6.168	-0.003	0.026	0.253	54.160	10.823	060.66
M6	6:338	8.503	0.017	0.125	9.465	7.186	0.031	0.028	0.111	54.841	12.268	98.915

Uncertaoint	Incertaointy due to Counting Statistics	ting Statistic	S							EPMA result Omphacite	Omphacite
1 sigma-relative	ıtive										
No.	Na20	FeO	Nb205	V203	AI203	MgO	MnO	K20	Ti02	Si02	CaO
In1	1.39	0.71	100	12.88	0.64	0.77	87.5	44.04	24.85	0.3	9.0
In2	1.37	0.7	100	12.73	0.65	0.8	100	143.62	29.41	0.3	0.61
In2b	1.38	0.68	97.24	10.55	0.64	0.81	109.88	33.96	20.3	0.3	0.61
In2c	1.36	0.7	98.69	12.35	0.63	0.8	90.85	41.73	28.04	0.3	0.61
ln3	1.4	0.67	100	14.33	99.0	0.82	43.55	48.71	31.92	0.3	0.62
In4	1.39	0.68	100	10.55	99.0	0.8	22.24	47.74	19.75	0.3	0.61
In 5	1.42	0.73	62.51	9.75	0.63	0.8	68.91	47.41	28.98	0.3	0.59
M1	1.4	0.77	70.71	24.7	0.62	0.76	17.39	23.91	80.23	0.29	9.0
M2	1.46	0.85	134.13	20.49	0.64	0.67	50.53	56.79	22.2	0.29	0.55
M3	1.47	0.87	714.14001	16.94	0.64	0.67	117	54.21	66.13	0.29	
M4	1.42	0.83	100	12.37	0.62	0.7	100	90.55	15.63	0.29	0.57
M5	1.35	0.71	201.25999	10.41	0.63	0.79	100	42.6	7.75	0.3	
M6	1.42	0.84	279.16	14.15	9.0	0.72	51.87	38.37	15.89	0.29	0.57

EPMA result	Rutile							
Unit: wt%								
No.	FeO	Nb2O5	V2O3	Al203	MnO	TiO2	SiO2	Total
ln1	0.75	-0.02	0.68	0.03	0.01	98.86	0.05	100.37
In2	0.64	0.05	0.95	0.01	0.00	99.77	0.01	101.42
In2b	0.62	0.00	1.25	0.03	0.01	99.46	0.00	101.37
In2c	0.73	0.05	0.70	0.00	0.01	99.93	0.01	101.44
In3	0.83	0.00	0.64	0.05	0.02	99.02	0.03	100.59
In4	0.60	-0.02	0.95	0.03	-0.02	99.90	0.04	101.48
In 5	0.83	0.05	1.03	0.03	0.00	98.83	0.03	100.80
M1	0.29	0.02	0.36	0.01	0.00	100.01	0.08	100.78
M2	0.34	0.08	0.56	0.05	0.00	99.25	0.06	100.34
M3	0.35	0.03	0.46	0.02	0.03	99.60	0.02	100.51
M4 (In)	0.52	0.06	0.46	0.00	0.02	100.59	0.04	101.69
M5 (In)	0.58	-0.03	1.04	0.01	-0.01	99.32	0.04	100.95
M6	0.41	0.02	0.60	0.03	-0.02	100.23	0.03	101.31

Uncertain	ty due to Co	ounting Sta	atistics			EPMA result	Rutile
1 sigma (re	elative)						
	FeO	Nb2O5	V2O3*	Al2O3	MnO	TiO2	SiO2
In1	3.83	100.00	3.50	37.07	159.58	0.20	24.58
In2	4.25	93.62	2.30	147.22	100.00	0.20	236.78
In2b	4.30	2689.58	1.40	38.77	244.16	0.20	494.28
In2c	3.90	83.94	3.40	100.00	169.63	0.20	90.15
In3	3.59	100.00	3.70	21.86	91.77	0.20	43.54
In4	4.47	100.00	2.30	41.10	100.00	0.20	30.01
In 5	3.52	82.23	2.00	39.29	100.00	0.20	48.54
M1	8.04	255.45	5.90	120.27	1530.67	0.20	16.62
M2	6.98	50.54	4.25	21.02	1050.42	0.20	22.37
M3	6.97	177.76	4.99	65.15	54.18	0.20	52.47
M4	4.60	100.00	1.94	84.97	100.00	0.20	32.23
M5	4.87	68.49	5.01	100.00	75.36	0.20	28.88
M6	6.05	247.58	3.97	39.35	100.00	0.20	41.11

^{. *} \it{V} uncertainties are calculated by using the function of Fe peak count rate

Appendix 7. Chemistry property data of the Franciscan sample obtained by LA-ICP-MS.

Sample(Omp)	SiO2 (Si)	Ti	٧	Cr	Cr	Zr	Nb	Та		V uncertainty (2 sigma)
	wt%	ppm	ppm	ppm	ppm	ppm	ppm	ppm	ppm	ppm
ln2	54	LOQ	475	830	LOQ	19	14	<0.22	C	32
In2b	54	LOQ	LOQ	767	LOQ	LOQ	LOQ	LOQ	LOQ	N/A
In2c	54	LOQ	491	954	LOQ	37	9	0	C	33
In3	54	LOQ	510	905	LOQ	LOQ	2	LOQ	LOQ	34
In5	54	LOQ	LOQ	1042	LOQ	LOQ	4	LOQ	C	N/A
M1	54	LOQ	352	775	LOQ	29	2	LOQ	LOQ	23
M2	54	LOQ	353	658	LOQ	LOQ	2	LOQ	LOQ	24
M3	54	LOQ	341	783	LOQ	25	2	LOQ	LOQ	23
M4	54	LOQ	504	906	134	142	3	LOQ	C	34
M5	54	LOQ	351	658	LOQ	13	2	LOQ	C	23
M6	54	LOQ	496	540	LOQ	27	3	LOQ	LOQ	33

Sample (Rt)	SiO2 (Si)	Ti	Ti	V	Cr	Cr	Zr	Nb	Та	V uncertainty (2 sigma)
	wt%	ppm	ppm	ppm	ppm	ppm	ppm	ppm	ppm	ppm
In2	LOQ	1208070	599500	2029	LOQ	LOQ	53	186	8	135
In2c	LOQ	1283823	599500	2035	LOQ	42	63	195	8	136
In4	LOQ	1252455	599500	1907	150	174	1030	132	5	127
M1	LOQ	1253377	599500	1556	62	75	51	270	20	104
M2	LOQ	1263172	599500	1535	43	51	60	208	16	102
M3	LOQ	1252169	599500	1525	37	57	43	265	16	102
M5	LOQ	1201255	599500	1483	35	48	82	222	12	99
M6	LOQ	1231578	599500	1471	79	95	63	206	10	98

Appendix 8. Chemistry property data of the Monviso sample obtained by EPMA.

EPMA Results	Omphacite	Unit: wt%								
No.	Na2O	FeO	TiO2	Al203	MgO	MnO	K2O	CaO	SiO2	Total
AL 3-1	5.52	8.28	0.21	6.23	9.47	0.10	0.01	14.38	54.26	98.46
AL 3-2	4.06	8.44	0.23	3.70	11.54	0.12	0.05	17.14	54.56	99.83
AL 2-1	3.61	8.60	0.01	2.71	12.28	0.11	0.03	18.15	54.58	100.09
AL 2-2	3.64	9.18	0.06	2.33	12.16	0.16	0.02	18.02	54.84	100.42
AL 4-1	3.49	7.79	0.06	3.20	12.17	0.09	0.04	18.20	54.54	99.58
AL 4-2	3.97	7.96	0.08	3.51	11.89	0.12	0.01	17.70	55.07	100.30
AL 5-1	5.35	11.77	0.00	4.10	9.43	0.12	0.02	14.46	54.62	99.88
AL 5-2	5.70	11.55	0.02	4.38	8.56	0.10	0.02	13.51	54.40	98.24
AL 1-1	5.33	11.68	0.00	5.30	8.49	-0.01	0.00	14.36	54.18	99.34
AL 1-2	4.86	8.55	0.02	5.68	10.11	0.06	0.02	14.56	55.00	98.85
UN 5-1	5.22	10.35	0.07	6.46	8.84	0.04	0.02	13.82	54.98	99.79
UN 5-2	5.43	11.57	0.13	5.71	8.46	0.03	0.01	14.14	54.51	99.98
UN 4-1	5.73	11.47	0.15	6.42	7.80	0.01	0.03	13.53	54.74	99.88
UN 4-2	5.45	12.27	0.00	5.33	8.19	0.02	0.02	14.07	54.77	100.14
UN 3-1	5.68	9.16	0.26	6.46	9.01	0.06	0.01	13.53	54.58	98.76
UN 3-2	5.72	10.97	0.53	6.56	8.09	0.01	0.03	13.63	54.85	100.39
UN 3-3	5.35	12.04	0.14	5.41	8.30	0.03	0.02	13.62	54.48	99.39
UN 3-4	5.72	12.27	0.12	5.84	7.70	0.04	0.00	13.38	54.77	99.83
UN 2-1	5.90	10.37	0.12	6.16	8.49	0.07	0.01	13.26	54.94	99.33
UN 2-2	4.54	12.30	0.21	3.42	9.74	0.01	0.01	16.35	54.03	100.60
UN 1-1	5.39	11.74	0.23	5.15	8.72	0.06	0.03	13.69	54.46	99.47
UN 1-2	6.67	11.30	0.30	7.56	7.26	0.10	0.02	11.13	54.82	99.17

_							*.*=				
Omphacite	Uncertainty	Due to Count	ing Statistics	(1 sigma)	Relative%						
No.	Na2O	FeO	TiO2	AI203	MgO	MnO	K20	CaO	SiO2		
AL 3-1	1.44	0.91	9.74	0.75	0.63	17.18	156.48	0.56	0.3		
AL 3-2	1.7	0.91	9.8	0.99	0.58	14.93	22.11	0.51	0.29		
AL 2-1	1.82	0.9	166.83	1.18	0.56	16.46	36.64	0.5	0.29		
AL 2-2	1.82	0.87	31.23	1.3	0.56	11.16	53.31	0.5	0.29		
AL 4-1	1.85	0.95	32.37	1.08	0.56	20.44	29.19	0.5	0.3		
AL 4-2	1.73	0.95	27.71	1.03	0.57	15.21	243.58	0.5	0.29		
AL 5-1	1.51	0.76	100	0.94	0.65	14.85	61.64	0.56	0.3		
AL 5-2	1.45	0.77	90.79	0.91	0.68	17.31	69.61	0.58	0.3		
AL 1-1	1.5	0.77	677.45001	0.83	0.69	100	100	0.56	0.3		
AL 1-2	1.56	0.91	92.13	0.79	0.62	28.34	52.52	0.56	0.3		
UN 5-1	1.51	0.82	30.29	0.74	0.67	42.68	74.69	0.57	0.3		
UN 5-2	1.49	0.77	17.4	0.79	0.69	60.76	83.66	0.57	0.3		
UN 4-1	1.45	0.78	14.19	0.74	0.72	219.23	42.68	0.58	0.3		
UN 4-2	1.49	0.75	100	0.82	0.7	71.37	76.96	0.57	0.3		
UN 3-1	1.44	0.87	8.56	0.74	0.66	27.04	108.01	0.58	0.3		
UN 3-2	1.45	0.79	4.85	0.73	0.7	204.96001	37.57	0.58	0.3		
UN 3-3	1.51	0.76	14.5	0.81	0.7	49.53	68.68	0.58	0.3		
UN 3-4	1.47	0.75	17.69	0.78	0.72	44.45	100	0.58	0.3		
UN 2-1	1.42	0.82	16.35	0.76	0.68	22.74	85.17	0.58	0.3		
UN 2-2	1.64	0.75	10.83	1.05	0.64	125.7	123.83	0.52	0.3		
UN 1-1	1.5	0.77	9.47	0.84	0.68	28.9	37.52	0.57	0.3		
UN 1-2	1.34	0.78	7.88	0.68	0.74	17.29	50.64	0.64	0.3		

Appendix 9. Chemistry property data of the Monviso sample obtained by LA-ICP-MS.

Unaltered	SiO2		CaO		Ti	Ti		V		Cr		Cr		Zr		Nb		Та		V u <u>nce</u>	rtainty
Omphacite		29		43	47		49		51		52		53		91		93		181		2 sigma
No.	wt%		wt%			ppm		ppm		ppm		ppm		ppm		ppm		ppm		ppm	
UN 1-1		55		13	PP	P P	226	P P	620	LOQ		LOQ		PP···		LOQ		ррии	0	рр	18
UN 1-2		55		13			209			LOQ		LOQ			0	-	n	LOQ			22
UN 2-1		55		11			148			LOQ		LOQ	125		-	LOQ	U	LOQ	0		22
UN 2-1		55		15		100	140			LOQ		100	123		0	-	0		0		26
		_		12		LOQ				_		LOQ			0		-		U		
UN 3-1		55 55				LOQ				LOQ		LOQ			-		U	LOQ	0		11
UN 3-4		55		13 13		LOQ				LOQ		LOQ				LOQ			0		12 23
UN 3-3						LOQ	222			LOQ		LOQ				LOQ		100	U		
UN 4-1		55		13			223			LOQ		LOQ		100	1	LOQ		LOQ	_		18
UN 4-2		55		13			200			LOQ		LOQ		LOQ		LOQ			0		18
UN 5-1		55		12			174			LOQ		LOQ		LOQ		LOQ			0		20
UN 5-2		55		14		LOQ			672	LOQ			88	LOQ			0		0		20
A + = =	C: 02		C-0		т:	т:		M		C:		C:-		7		NII-		T-			and and an also a
Altered	SiO2		CaO		Ti	Ti		V	Г4	Cr		Cr		Zr	04	Nb		Та		v unce	rtainty
Omphacite		29		43	47		49		51		52		53		91		93		181		2 sigma
No.	wt%	-	wt%	_	ppm	ppm		ppm	160	ppm	F762	ppm		ppm		ppm		ppm		ppm	
AL 5-1		55			LOQ		230		168		5762		5862			LOQ			0		5
AL 5-2		55		_	LOQ		188		124		3760		3788		0		0		0		4
AL 1-1		55		_	LOQ		156			LOQ		LOQ			1		0		0		27
AL 1-2		55			LOQ		166			LOQ		LOQ			1		0		0		22
AL 4-2		55		_	LOQ		217		649		408		404			LOQ			0		19
AL 4-1		55		15	LOQ		201		712		219		256		0	LOQ			0		21
AL 2-1		55		16	LOQ		249		524		1095		1139		1		0		0		15
AL 2-2		55		17	LOQ		291		290		741		779		1	LOQ			0		9
AL 3-1		55		15	N/A	1	1236		600		407		417		2	LOQ			0		18
AL 3-2		55		18	N/A		241		657		352		369		3		0		0		19
Unaltered	SiO2		CaO		Ti	Ti		V		Cr		Cr		Zr		Nb		Ta		V unce	rtainty
Rutile		29		43	47		49		51		52		53		91		93		181	2 sigma	a
No.	wt%		wt%		ppm	ppm		ppm		ppm		ppm		ppm		ppm		ppm		ppm	
UN 1-2	LOQ		LOQ		N/A	59	0000		1797	LOQ			175		29		103		7		53
UN 1-1	LOQ		LOQ		N/A	59	0000		1844	LOQ			213		40		95		7		54
UN 2-1	LOQ		LOQ		N/A	59	0000		1980		452		449		14		40		2		58
UN 2-2	LOQ		LOQ		N/A	59	0000		2084		486		415		17		54		2		61
UN 4-2	LOQ		LOQ		N/A	59	9000		2307	LOQ		LOQ			28		60		5		68
UN 5-1	LOQ		LOQ		N/A	59	9000		2379		299		266		31		78		4		70
UN 5-2	LOQ		LOQ		N/A	59	9000		2404		474		505		26		71		3		71
Altered	SiO2		CaO		Ti	Ti		V		Cr		Cr		Zr		Nb		Та		V unce	rtainty
Rutile		29		43	47		49		51		52		53		91		93		181	2 sigma	a
No.	wt%		wt%		ppm	ppm		ppm		ppm		ppm		ppm		ppm		ppm		ppm	
AL 5-2	LOQ		LOQ		1484054		9000		1033		797		767		20		6		0		30
AL 1-2	LOQ		LOQ		1559588	59	9000		1299		1151		1112		25		45		1		38
AL 4-1	LOQ		LOQ		1518617	_	9000		984		553		614		85		20		1		29
	LOQ		LOQ		1504868		9000		1081		1962		2241		18		33		1		32
AL 2-1				_													_		_		32
AL 2-1 AL 2-2	LOO		LOO		1563623	5.9	9000		1083		2006		2059		45		34		1		3/
AL 2-1 AL 2-2 AL 3-1	LOQ		LOQ LOQ	-	1563623 N/A		9000 0000		1083 1049		2006 1008		2059 1195		45 25		34 52		1		31

Appendix 10. Academic Integrity.

"I pledge on my honor that I have not given or received any unauthorized assistance on this assignment/examination."